BETA-DELAYED PARTICLE EMISSION, A > 70

B. Jonson*), E. Hagberg**), P.G. Hansen†), P. Hornshøj††) and P. Tidemand-Petersson
The ISOLDE Collaboration, CERN, Geneva, Switzerland.

Abstract

Experiments on delayed particle emission are reviewed, with special emphasis on the recent alpha and proton data. Interpretations of the results within the framework of the statistical model are given, and the fluctuations in the spectra are shown to provide an experimental tool for measuring level densities in nuclei far from stability.

## 1. Introduction

The area of the nuclear chart within reach of experimental nuclear-structure physics has widened considerably in recent years -- mainly owing to the rapid development of in-beam and on-line systems. These specialized techniques have helped us to overcome some of the main experimental difficulties such as, for example, short half-lives and small formation cross-sections. We may mention that nuclides with half-lives in the 100 msec region and with formation cross-sections as low as 1 nb are within reach in high yields[1]. The new nuclides far from stability that now can be studied differ in many respects from those in regions closer to stability; for example, the abnormal neutron to proton ratio, the asymmetry in the binding of the two types of nucleons, and the increasing isobaric mass difference which gives a high energy available for the beta decay. Besides alpha, beta, and gamma radiations, new modes of radioactive decay become possible as beta-delayed particle emission, beta-delayed fission, and Coulomb-delayed proton emission. In this paper we shall present experimental results and interpretations of delayed particle emission from nuclei with A > 70. Before starting on this, we shall first discuss some of the main features of the nuclei under consideration.

## 2. High-energy beta decay

Let us choose $^{118}$Cs as a "typical" nucleus far from stability. A schematic decay scheme of this nucleus is shown in Fig. 1. The energy available for beta decay is close to 10 MeV, and the first excited state in the daughter nucleus, $^{118}$Xe, has an energy of 338 keV [2,3]. The spacing between levels becomes progressively smaller and smaller with increasing excitation energy. The predicted[4,5] average spacing of, for example, $3^+$ states is about 6 keV at 5 MeV, while it is only 10 eV at the top of the excitation spectrum. The channels open for the beta decay are spread from the ground state to the highest energies over all the states permitted by the selection rules. A rough estimate gives around $10^5$ possible final states for allowed beta transitions (with an assumed spin parity of $3^+$ for the ground state of $^{118}$Cs). The predicted proton separation energy ($B_p$) in $^{118}$Xe is 4.9 MeV, and an alpha particle is unbound with about 1.5 MeV. High-lying states in $^{118}$Xe are therefore expected to show proton and alpha emission in competition with gamma de-excitation. Both of these decay modes have been observed experimentally[6-9].

The nature of the dense states in the high excitation regions is very complicated, and a good starting point for their description is in terms of averages and statistical nuclear reaction theories[10]. The total widths of the resonances relevant to this discussion are much smaller than the average level spacing. We are thus concerned with individual states of the same type as the resonances observed in the neutron capture process. The individual transition probabilities and the level spacings show pronounced local fluctuations, and the most convenient approach is then to treat only averages over a

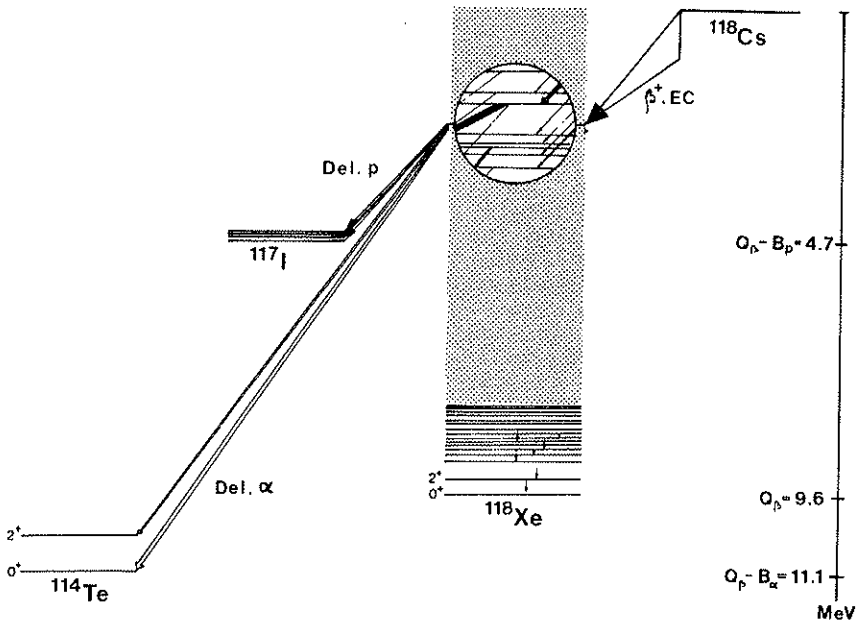


Fig. 1 Decay scheme for $^{118}$Cs.

*) Visitor from the Dept. of Physics, Chalmers Univ. of Technology, Göteborg, Sweden.
**) Dept. of Physics, Chalmers Univ. of Technology, Göteborg, Sweden.
†) On leave from the Inst. of Physics, Univ. of Aarhus, Aarhus, Denmark.
††) Inst. of Physics, Univ. of Aarhus, Aarhus, Denmark.

large number of states. A very useful quantity is the *strength function* defined[11] as

$$S_{\lambda c} = (\gamma^2_{\lambda c})\ \rho_\lambda \ ,$$

where $\gamma^2_{\lambda c}$ denotes the square of the overlap integral between two sets of nuclear wave functions, $\rho_\lambda$ the level density of the states $\lambda$, and c the possible exit channels. The overlap integrals are normally referred to as reduced widths since they are factors of the observed partial widths $\Gamma_{\lambda c} = 2P_c\gamma^2_{\lambda c}$ [10]. The factor $2P_c$ is the barrier penetrability in the exit channel. For the beta decay a convenient definition of the strength function has been given[12,13] as the energy distribution of the reciprocal ft value,

$$S_\beta(E) \equiv b(E)/\left[f(Z,Q_\beta\text{-}E)\cdot T_{\frac{1}{2}}\right] \ ,$$

where b(E) is the absolute beta intensity per MeV of states at excitation E, $Q_\beta$ is the energy available for beta decay, $T_{\frac{1}{2}}$ the beta half-life in seconds, and f(Z,Q-E) is the statistical rate function. Experimental determinations of beta strength functions, based on measurements with a total absorption spectrometer with large NaI(Tl) crystals, have been performed at ISOLDE for $\beta^+$, EC decay[12,14] and at OSIRIS in Studsvik for $\beta^-$ emitters[15-17]. Figure 2 illustrates some results from these measurements.

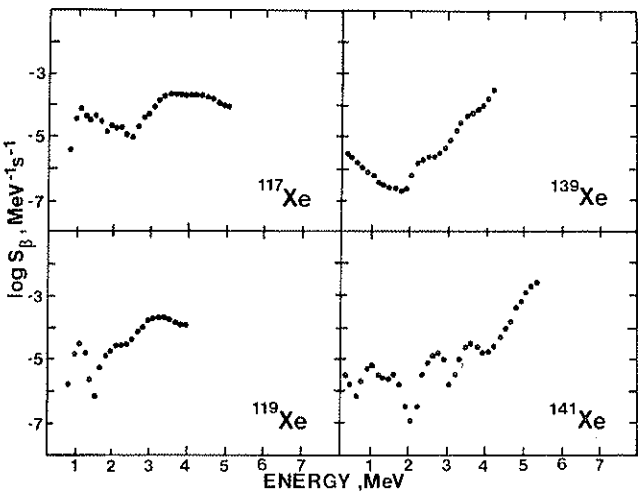


Fig. 2 Beta strength functions from $^{117,119}$Xe (Ref. 14) and $^{139,141}$Xe (Ref. 16). The strength functions were obtained from unfolding of total absorption gamma spectra measured with two large NaI(Tl) crystals. Note the marked difference in the energy behaviour of the strength on the two sides of stability: on the neutron-deficient side the strength is more or less constant, while the neutron-rich isotopes show a steep increase in the strength towards higher energies.

The most successful theory for high-energy beta decay is the "gross theory" developed by Yamada and Takahashi[18-20]. In their approach they combine a simplified single-particle model with a superimposed giant resonance behaviour and determine the absolute strength with the use of sum rules. The gross theory has been shown[20] to be in qualitative agreement with the experimental data.

There is a great similarity between beta strength and, for example, proton and alpha strength functions. In both cases we are concerned with overlap integrals between initial and final states with a relatively slow variation in energy. Collective effects, however, play a significant role in both beta and gamma strengths[13,21], while single-particle models describe the major features of the proton, neutron, and alpha strengths. The delayed particle data provide us with information that is important for a further understanding of both the beta strength functions and the particle strength functions of nuclei far from the region of beta stability.

The strength functions describe the average behaviour of the nucleus over many final levels at a given excitation energy. The individual transition probabilities and the spacings between the states have wide distributions, and the finite number of resonances contributing to the average will then give rise to *fluctuations* in the observed intensity. Such fluctuations have been observed in the slow-neutron average cross-sections[22], and they are also the origin of the fine structure observed in the delayed particle spectra. The fluctuations provide us with an experimental tool for measuring nuclear level densities. The increasing body of high-resolution data on delayed particle emission will thus make possible a systematic investigation of level densities in nuclei far from stability.

## 3. Experimental studies of delayed particle emission

The necessary condition for a nuclide to be a precursor for delayed particle emission is that the energy available for the beta decay exceeds the particle separation energy in the daughter nucleus. This condition already becomes fulfilled throughout the whole nuclidic chart for nuclides lying several mass numbers from the nucleon drip lines. On the neutron-rich side of stability, we may observe beta-delayed neutron emission, while for neutron-deficient precursors the corresponding decay mode gives proton and (or) alpha emission. Effectively there is a minimum value of the Q value for particle emission below which the branching ratio becomes too small for an experimental observation of the delayed particle phenomenon. This is most pronounced for the charged particle emission since the Coulomb barrier reduces the transmission coefficients considerably at low energies. This results in a complete domination of the gamma channel. An example is found in the data from the mercury precursors where protons with energies below 3 MeV are not observed, while a typical energy spectrum in the krypton region starts below 1 MeV. The predicted number of experimentally observable precursors for delayed particle emission exceeds 1000. A fair amount of these nuclides are available or will be available for experimental studies in the near future.

### 3.1 Neutron-deficient precursors

The first artificially produced precursors in the heavy mass region were found in the decay of light tellurium isotopes[23-26]. The two isotopes $^{109,111}$Te were identified as delayed proton emitters, and the observed energy spectra showed broad energy distributions. At the Leysin Conference, six new cases in xenon and mercury were reported[27]. During the six years which have passed since then there has been a rapid increase in the available data, and we have now information including spectral shapes, absolute intensities, and fine structure, feeding to excited final states and $Q_\beta$-$B_p$ values. An up-to-date summary of the present knowledge is given in Table 1 [6-9,23-53].

Table 1

Beta-delayed proton emitters in nuclei with A > 70

| Nuclide | $T_{\frac{1}{2}}$ (sec) | Exp. final levels a) (MeV) | Exp. proton branching ratio | Exp. b) $Q_\beta - B_p$ (MeV) | Del. protons / Del. alphas c) | References |
|---|---|---|---|---|---|---|
| $^{73}$Kr | 22 ±4<br>25.9±0.6 | 0.00(65%)<br>0.862(35%) | $(6.8\pm1.2)\times10^{-3}$ | 4.85±0.30 | - | 28,29,30,31 |
| $^{109}$Te | 4.2±0.2 | d) | d) | 7.14±0.10 | - | 23,24,25,26,<br>32,33,34,35,36 |
| $^{111}$Te | 19.0±0.7 | d) | d) | 5.07±0.07 | - | 23,26,32,33,34<br>37,38,39,40 |
| $^{113}$Xe | 2.8±0.2 | d) | d) | d) | - | 41 |
| $^{115}$Xe | 18 ±4 | 0.0(42%)<br>0.709(58%)<br>1.484(<2%) | $(3.4\pm0.6)\times10^{-3}$ | 6.20±0.13 | - | 27,42,43,44 |
| $^{117}$Xe | 65 ±6 | 0.0(86%)<br>0.679(14%) | $(2.9\pm0.6)\times10^{-5}$ | 4.1±0.2 | - | 27,42,43,44 |
| $^{114}$Cs | d) | d) | d) | d) | 33±12 | 9,45 |
| $^{116}$Cs e) | 3.5±0.2 | 0.055<br>0.107<br>0.318<br>0.580<br>0.590 | $(2.7\pm0.4)\times10^{-3}$<br>$(3\pm1)\times10^{-3}$ | 6.4±0.3<br>6.45±0.3 | 51±5 | 6,7,9,45,46,47,<br>48,49 |
| $^{118}$Cs | 16.4±1.2 | 0.117<br>0.160<br>0.221 | $(4.2\pm0.6)\times10^{-4}$ | 4.7±0.3 | 17.2±0.3 | 6,7,8,9,45,46 |
| $^{120}$Cs | 58.3±1.8 | d) | $(7\pm3)\times10^{-8}$ | d) | 0.36±0.10 | 6,7,8,9,45,46 |
| $^{119}$Ba | 5.4 ±0.3 | d) | d) | 6.2±0.2 | - | 48,49,50 |
| $^{121}$Ba | 29.7±1.5 | d) | $\sim 2.5\times10^{-4}$ | 4.2±0.3 | - | 48,49 |
| $^{129}$Nd | 6 ±3 | d) | d) | d) | - | 51 |
| $^{131}$Nd | 22 ±6 | d) | d) | d) | - | 51 |
| $^{133}$Sm | 3.2±0.4 | d) | d) | d) | - | 51 |
| $^{135}$Sm | 10 ±2 | d) | d) | d) | - | 51 |
| $^{179}$Hg | 1.09±0.04 | d) | $\sim 2.8\times10^{-3}$ | d) | - | 27,42,43,44 |
| $^{181}$Hg | 3.6 ±0.3 | 0.0(50%)<br>0.158(50%) | $(1.8\pm0.5)\times10^{-4}$ | d) | $(1.5\pm0.6)\times10^{3}$ | 27,42,43,44,52 |
| $^{183}$Hg | 8.8 ±0.5 | d) | $(3.1\pm0.7)\times10^{-6}$ | d) | - | 27,42,43,44 |

a) From delayed-proton gamma coincidences.
b) From 511 keV (or positron) delayed proton coincidences.
c) See also Table 2.
d) Not determined.
e) Measurements on high-energy beta-rays have shown that $^{116}$Cs has an isomer with $T_{\frac{1}{2}} < 1$ sec (Ref. 53). The delayed proton activity shows only one component (3.5 sec).

Table 2

Beta-delayed alpha emitters in nuclei with A > 70

| Nuclide | $T_{\frac{1}{2}}$ (sec) | α/dis. | Del.p/Del.α | References |
|---|---|---|---|---|
| $^{76}$Rb | 36.8±1.5 | $(3.8\pm1.0)\times10^{-9}$ | - | 9,45 |
| $^{114}$Cs | a) | a) | 33±12 | 9,45 |
| $^{116}$Cs | 3.5±0.2 | $(6\pm1)\times10^{-5}$ | 51±5 | 9,45 |
| $^{118}$Cs | 16.4±1.2 | $(2.4\pm0.4)\times10^{-5}$ | 17.2±0.3 | 8,9,45 |
| $^{120}$Cs | 58.3±1.8 | $(2.0\pm0.4)\times10^{-7}$ | 0.36±0.10 | 8,9,45 |
| $^{181}$Hg | 3.6±0.3 | $(9\pm3)\times10^{-8}$ | $(1.5\pm0.6)\times10^{3}$ | 52 |
| $^{212}$Bi | 3600 | $1.4\times10^{-4}$ | - | 54 |
| $^{214}$Bi | 1188 | $3\times10^{-5}$ | - | 54 |

a) Not determined.

The alpha particle is unbound in the ground state for most neutron-deficient nuclei with Z > 50, and ground-state alpha emission is a common decay mode above N = 84. The energy available for delayed alpha emission is typically several MeV for the neutron-deficient nuclei, and this decay mode is thus expected to occur regularly together with proton emission. The first cases of this type have been reported within the last year[8,9,52]. A summary of the present results is given in Table 2 [8,9,45,52,54].

A few typical experiments will be discussed below as an illustration of the experimental techniques and the available data.

3.1.1 Measurements of singles spectra. Figure 3 shows the delayed proton and alpha spectra from $^{116}$Cs (Ref. 45) measured with a ΔE-E counter telescope. The radioactive beam of $^{116}$Cs ions was directed into the experimental set-up and intercepted by a 20 μg/cm² carbon foil placed in front of

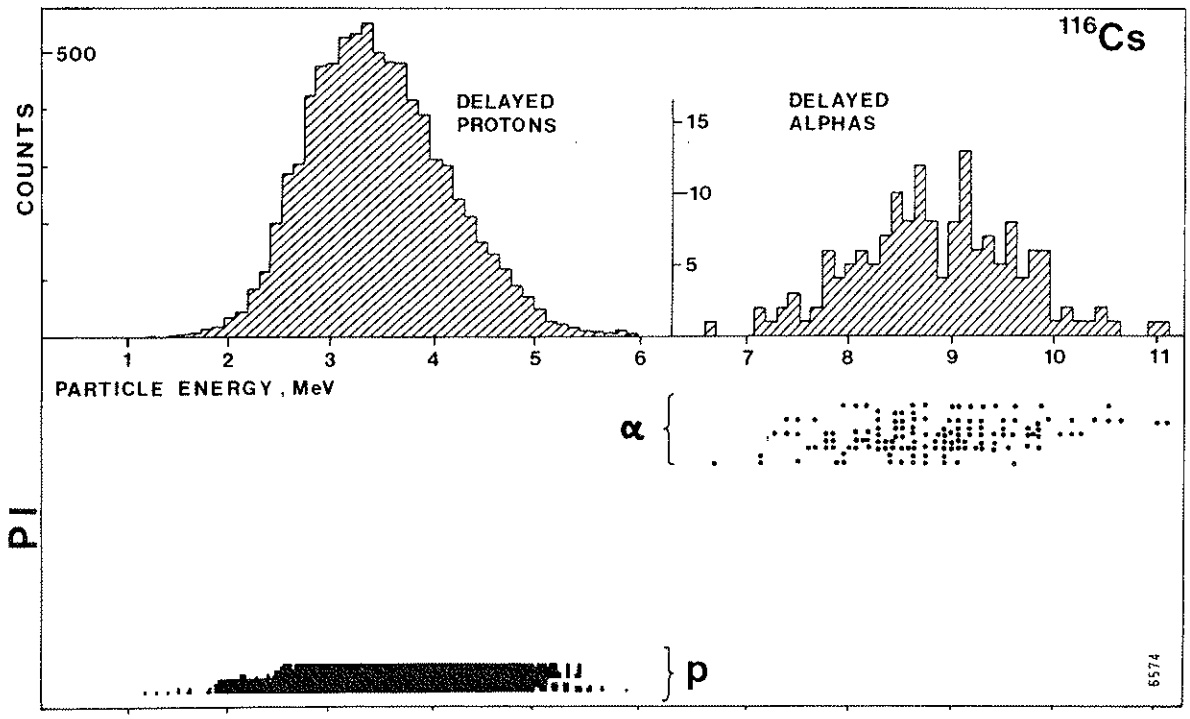


Fig. 3 Delayed proton and alpha spectra from $^{116}$Cs. The Cs activity was produced at the ISOLDE facility in a $^{139}$La(p,3p2n)$^{116}$Cs spallation reaction with 600 MeV protons from the CERN Synchro-cyclotron (Ref. 1). The particle counting was performed with a ΔE-E detector telescope equipped with surface barrier detectors (ΔE: 25 μm, 100 mm², E: 500 μm, 450 mm²). The lower part shows the two-dimensional spectrum of particle energy versus particle identifier signal (PI), and the upper part the integrated delayed proton and delayed alpha spectra. The branching ratios are (2.7 ± 0.4) × $10^{-3}$ and (6 ± 1) × $10^{-5}$ for the delayed proton and alpha activities, respectively.

the detector system. Signals for particle identification and energy were stored two-dimensionally so that both proton and alpha events were recorded. The total number of atoms collected during the experiment was found from absolute counting of residual activity of 2.5 h $^{116}$Te (Ref. 55) on the collector foil. The proton and alpha branching ratios were then determined to be $(2.7 \pm 0.4) \times 10^{-3}$ and $(6 \pm 1) \times 10^{-5}$, respectively.

The delayed proton spectrum from $^{119}$Ba shown in Fig. 4 was measured by Karnaukhov and his collaborators[48] at the BEMS-2 isotope separator[56] in Dubna. The proton counting was performed with a singles detector. The increase in the intensity at the low-energy part of the spectrum is due to beta particles from the decay of $^{119}$Ba and its daughters. One distinctive feature, common for the delayed particle spectra, is demonstrated in this case; the

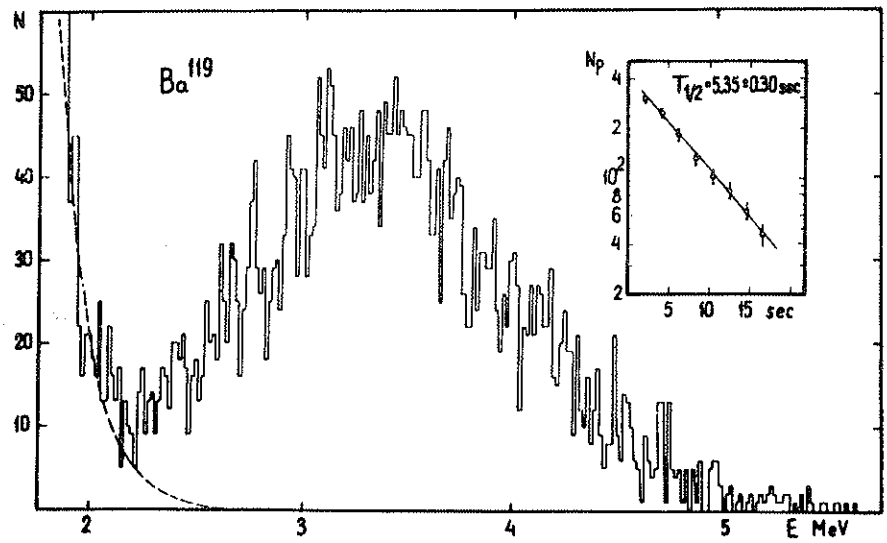


Fig. 4 The energy spectrum of beta-delayed protons from $^{119}$Ba (Ref. 48). The Ba activity was produced in a $^{90}$Zr($^{32}$S,3n) reaction in a target of 2 mg/cm$^2$ Zr bombarded with 158 MeV $^{32}S^{5+}$ ions from the JINR heavy ion accelerator. The protons were detected in a silicium detector, and the experimental resolution was 40 keV FWHM. The inset in the figure shows the result of a half-life measurement for $^{119}$Ba as determined from counting of protons.

observed energy distribution shows a broad hump over a few MeV in energy with almost no developed fine structure.

3.1.2 Emulsion experiments. The delayed particle activity offers the easiest distinguishable radiation for the identification of extremely neutron-deficient nuclei in regions where there is no ground-state alpha emission. As a more sensitive alternative to the detection of particles with a counter telescope, a technique based on nuclear emulsions as detecting elements has been used[41]. In these experiments the emulsion is placed in a lead shielding inside the collector tank of the isotope separator. Several ion beams might enter through a slit in the lead shielding (Fig. 5) and are then collected on a rotating disk whose active side moves close to the emulsion surface. After development of the plates, the proton and alpha tracks can easily be distinguished from the beta- and gamma-fogging of the emulsion. The half-life of the delayed particle precursor is obtained from the track density as a function of the distance from the collecting position. The emulsion arrangement offers a large solid angle (close to $2\pi$) and a check on the background in the regions between the masses. The method is especially powerful for the identification of nuclei produced in extremely low yields. The very high sensitivity of this technique permitted the first detection of the two delayed proton emitters $^{113}$Xe (Ref. 41) and $^{116}$Cs (Ref. 46). As an example of the emulsion data, Fig. 5 displays the energy spectrum of delayed protons from $^{113}$Xe determined from measurements of the proton track lengths in an Ilford K2 nuclear emulsion. The inset in the figure shows the half-life curve which gives the value $T_{\frac{1}{2}} = 2.8 \pm 0.2$ sec for $^{113}$Xe. Such information from nuclei very far from stability provide us

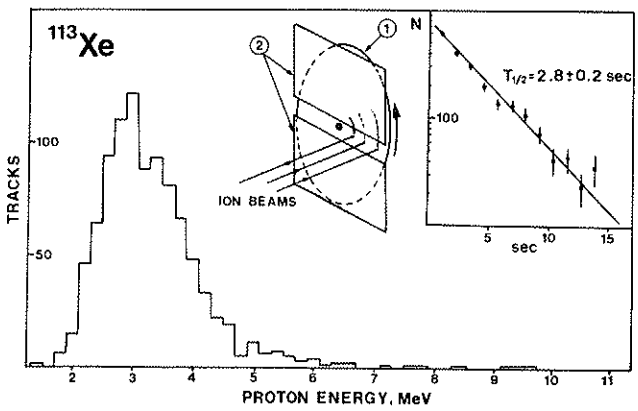


Fig. 5 The delayed proton spectrum from $^{113}$Xe measured by the emulsion method. The rotating disk collector was placed inside the collector chamber of the isotope separator. Mass-separated ion beams of Xe isotopes are collected on a disk (1) of stainless steel. The proton events were detected in 400 μm Ilford K2 emulsion plates (2). The whole arrangement was shielded by 2 cm of lead. The inset shows the half-life measured from the track density as a function of time. N is the number of proton tracks/0.26 radians corresponding to a counting time of 1.13 sec per point.

with an important check of the beta half-lives predicted from the gross theory[57]. The comparison between the calculations and the experimental data for Xe isotopes shown in Fig. 6 testifies the usefulness of this theory.

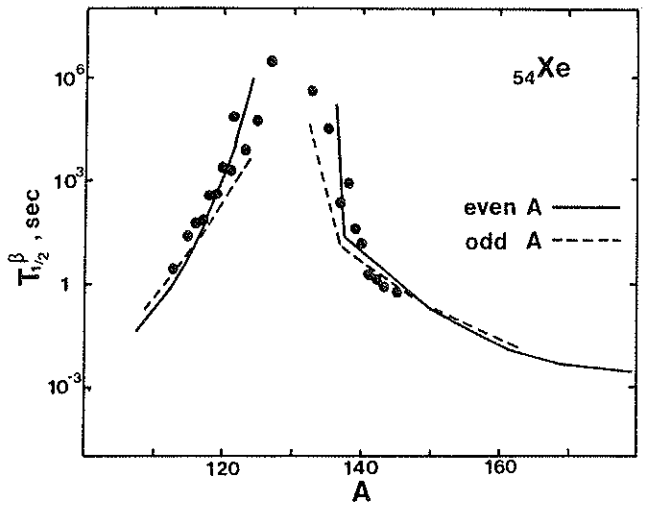


Fig. 6 Beta decay half-lives of xenon isotopes calculated from the gross theory[57] (full drawn and dotted lines). The points indicate the experimental half-lives.

3.1.3 Coincidence experiments. Several delayed particle emitters are produced in intensities high enough to make more sophisticated experiments possible, as for example particle-gamma coincidence experiments. The gamma spectra shown in Fig. 7 were detected in a 40 cc Ge(Li) detector in coincidence with delayed protons from $^{116}$Cs and $^{118}$Cs. The gamma energies observed in these spectra correspond to transitions in the delayed proton daughters $^{115}$I and $^{117}$I (Refs. 58 and 59), respectively. The relative feeding to excited final states is predicted in the statistical model calculations of the delayed particle spectra[60], and the experimental results are of great importance as a test of this model. The 511 keV peak, representing coincidences between protons and annihilation radiation from positrons feeding the proton-emitting states, may be used to calculate the $Q_\beta$-$B_p$ value[44]. The intensity of the 511 keV peak in the $^{116}$Cs spectrum corresponds to a 40 ± 8% $\beta^+$-branch, and the $Q_\beta$-$B_p$ value is then determined to 6.45 ± 0.30 MeV. This result is in excellent agreement with the value 6.4 ± 0.3 MeV obtained from counting of positron-proton coincidences[49]. The $Q_\beta$-$B_p$ values measured until now are included in Table 1.

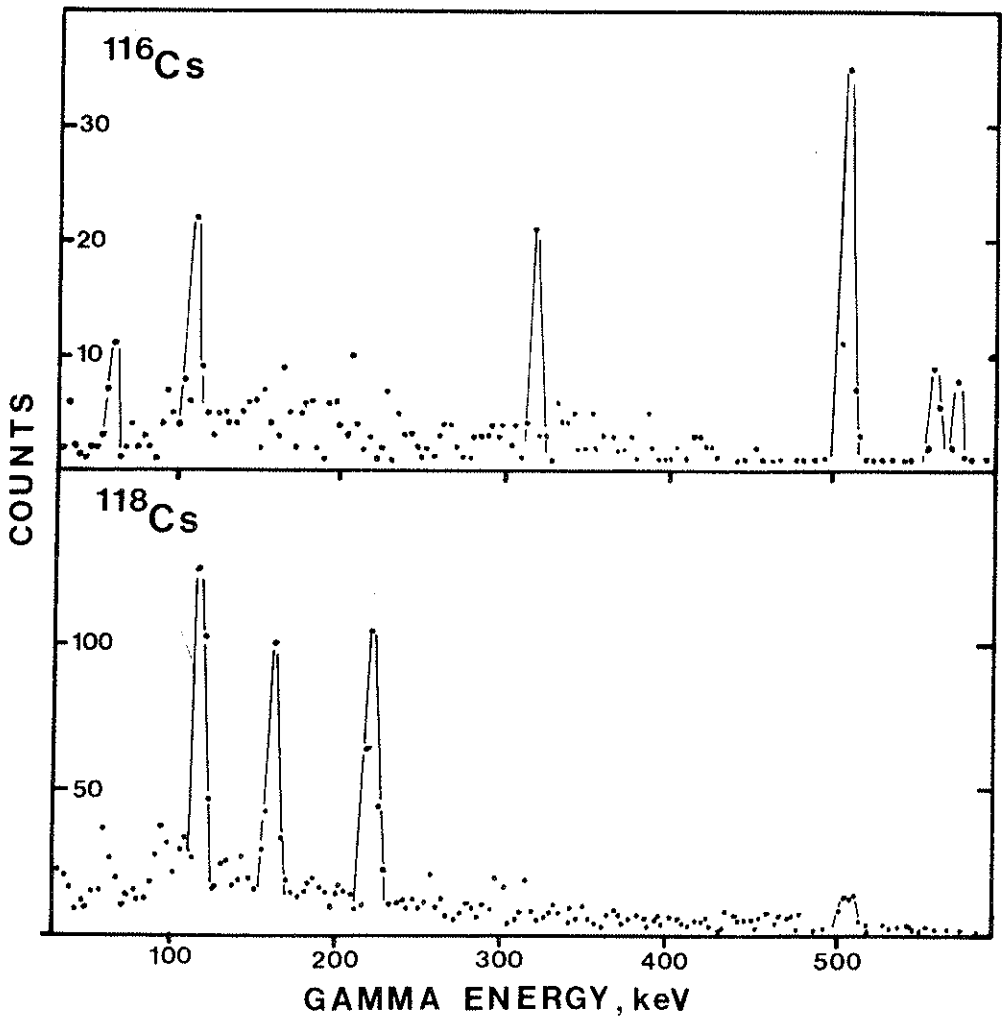


Fig. 7 Spectra of gamma-rays in coincidence with delayed protons for $^{116,118}$Cs. A 100 μm, 100 mm$^2$ surface-barrier detector was used as proton detector and a Ge(Li) detector for the gamma-rays. The $^{116}$Cs spectrum shows coincidences with annihilation radiation and gamma-rays in $^{115}$I with energies 55, 107, 318, 580, and 590 keV. The three gamma lines in the $^{118}$Cs spectrum correspond to the three transitions 117, 160, and 221 keV in $^{117}$I (Refs. 58 and 59). The positron to proton ratios are 40 ± 8% and 2.1 ± 0.5%, which gives (Refs. 45 and 7) $Q_\beta - B_p$ = 6.45 MeV and 4.7 MeV for $^{116}$Cs and $^{118}$Cs, respectively.

A first systematics of the difference of $Q_\beta$-$B_p$ has been given by Bos et al.[61] where they predict this parameter for most elements. The experimental data have helped in the systematics, and the coincidence results may be combined with values obtained from fits to the end points of the particle spectra (see next section) to extract information about the individual parameters.

An attempt to observe the delayed alpha branch from $^{118}$Cs to the $2^+$ state [709 keV [62]] in $^{114}$Te has been made. In this experiment, 1100 delayed alpha particles were counted[45], and the number of coincidences with the 709 keV gamma energy were found to be less than 5. This gives an upper limit to the feeding of the 709 keV state of 50%.

### 3.2 Neutron-rich precursors

On the neutron-rich side of stability, delayed neutron emission occurs. This process is analogous to delayed proton emission and may be understood in the same terms as this process. Many precursors for delayed neutron emission have been identified [see e.g. the compilation by Tomlinson[63]], and they have been studied extensively because of their importance to nuclear reactors and their role in astrophysical theories. The experimental data include half-life determinations for the precursors and measurements of neutron branching ratios. Measurements of spectral shapes have been performed in a number of cases[64-67], and the high resolution of the $^3$He proportional counters has given a possibility to study the fine structure in the delayed neutron spectra. An interpretation of some of these data is given in another contribution[68] to this conference. As an example of the data, Fig. 8 shows the energy spectrum of delayed neutrons from $^{93}$Rb (Ref. 67).

Neutron counting has also been shown to offer a very sensitive method for half-life determinations on the extreme neutron-rich side of stability. Recent measurements at Studsvik[69] have given new and improved half-lives for a number of Zn, Ga, Br, and Rb isotopes.

The main data on delayed neutron emission come from measurements on nuclides situated in the regions close to the two mass peaks of thermal fission products. Only very limited data from heavier precursors exist[63], and it might therefore be of interest to mention that some new targets for high-energy proton reactions are expected to give activities also far out on the neutron-rich side. An example[70] is the heavy thallium isotopes produced in a target of, for example, uranium. It would be very interesting to complete the information from the lighter regions with data from such heavy precursors.

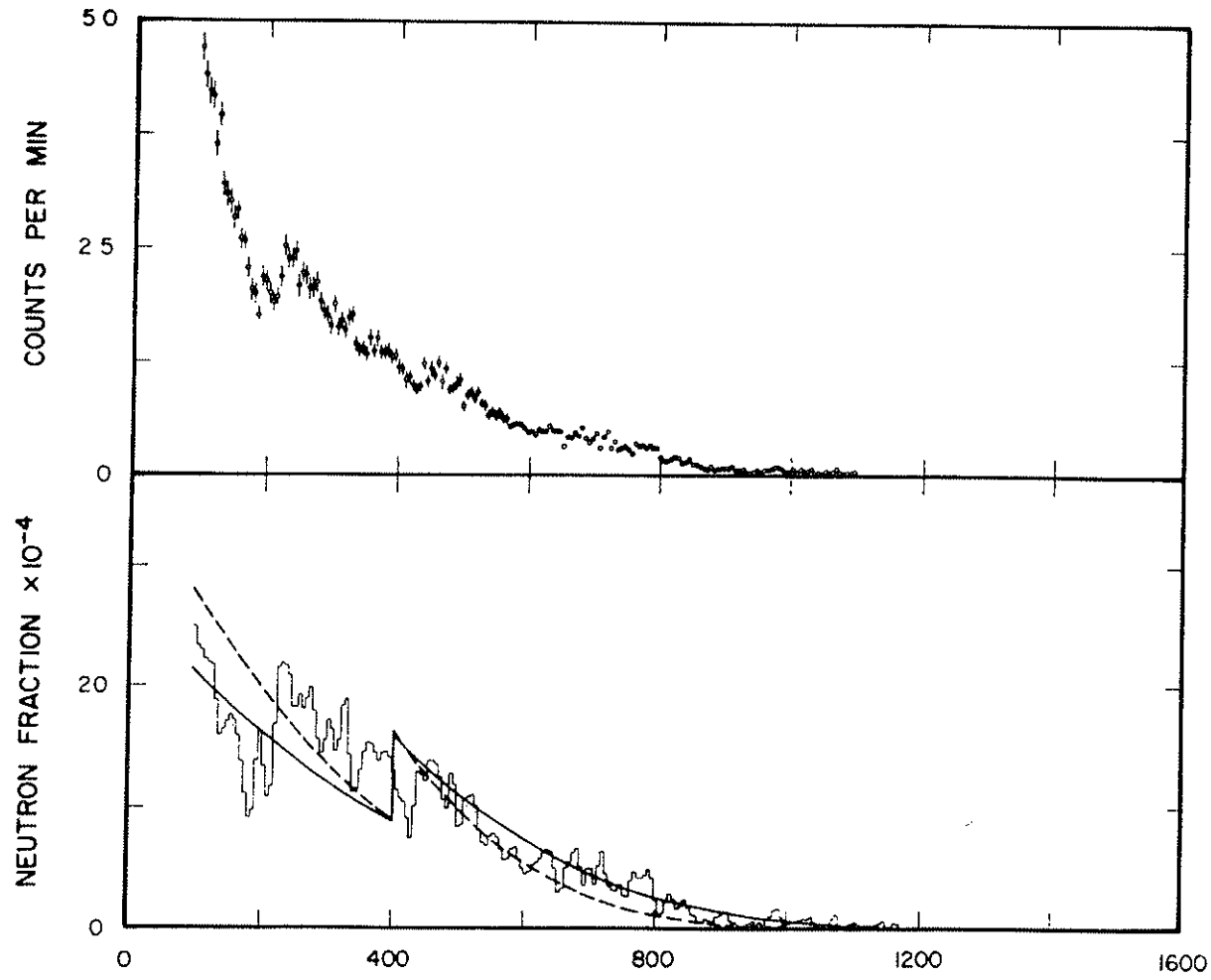


Fig. 8 Energy spectrum of beta-delayed neutrons from $^{93}$Rb measured with a $^3$He proportional counter at the OSIRIS facility at Studsvik. The lower part shows the unfolded spectrum (histogram) corrected for efficiency. The curves show the calculated envelopes for different assumed mass data (Ref. 67).

### 3.3 Beta-delayed fission

For very heavy nuclides the fission barrier becomes sufficiently low to give an energetic possibility of beta-delayed fission. This process is expected to occur on both sides of stability, but until now there are only very limited experimental results. The only reported cases are the fission activities observed at JINR in Dubna in the reaction products following irradiation of $^{209}$Bi with $^{22}$Ne [71] and $^{230}$Th with B-ions[72,73]. These activities have been explained[74] as beta delayed fission of $^{227,229}$Np and $^{232,234}$Am.

Like the delayed neutron process, beta-delayed fission plays an important role in the r-process calculations[21,75,76]. This will be discussed in the contribution by Wene[77] to this conference.

## 4. Statistical model calculations of delayed particle spectra

Calculations of delayed proton spectra in a statistical approach have been outlined by Hornshøj et al.[60]. The main features of the experimental results, as spectral shapes, absolute intensities, and feeding to excited final states, could be understood from such a model. Corresponding calculations for delayed neutron emission have been performed by Pappas and Sverdrup[78]. All of these calculations contain more or less the same ingredients, and in the following a summary of the main underlying ideas is given.

The particle-emitting states have excitation energies that are so high that one expects the compound nucleus description to be applicable. The statistical theory of nuclear reactions is then relevant (see, for example, Ref. 10). The delayed particle process is depicted as proceeding in two stages:

i) The primary beta-decay, which populates closely spaced excited levels, and

ii) the subsequent decay of an excited level where the evaporation model is used. This model assumes that the decay of the compound nucleus is completely independent of the way in which the excited level was formed.

The calculation of the beta intensity must include some assumption of the shape of the beta strength function $S_\beta$. From this and the statistical rate function for beta decay, we obtain the intensity distribution as a function of the excitation energy E in the daughter nucleus as

$$b(E) = S_\beta(E)\cdot f(Z,Q_\beta-E) / \int_0^{Q_\beta} S_\beta(E) f(Z,Q_\beta-E)\, dE, \quad (4.1)$$

where $Q_\beta$ is the energy available for the beta decay. The weight factor for feeding of intermediate states, with spin and parity $I_i^{\pi i}$, from an initial state $I^\pi$, may be approximated[60] as

$$\omega(I,I_i) = \frac{2I_i+1}{3(2I+1)} . \quad (4.2)$$

The compound nucleus expression for the particle intensity to a final level f is then given as

$$I_x^{if}(E_x) = \omega(I,I_i) b(E) \frac{\Gamma_x^{if}(E_x)}{\Gamma_{tot}^i} , \quad (4.3)$$

where $E_x$ is the energy of the emitted particle x, and $\Gamma_x^{if}(E_x)$ the partial width for a transition between the initial state $|i)$ and the final state $(f|$. The particle energy $E_x$ is related to the excitation energy E, as

$$E = B_x + E_f + \frac{A}{A-M_x} E_x \quad (4.4)$$

where $B_x$ is the particle separation energy in the intermediate nucleus, $E_f$ the excitation energy of the final state, and $M_x$ the mass of the emitted particle. The total width $\Gamma_{tot}^i$ is the sum of the total gamma width and the partial widths of all open particle channels. The expression for the total width when, for example, proton and alpha emission is energetically possible, then becomes

$$\Gamma_{tot}^i = \Gamma_\gamma^i + \sum_{f'} \Gamma_p^{if'}(E_p') + \sum_{f''} \Gamma_\alpha^{if''}(E_\alpha'') , \quad (4.5)$$

where f′ and f″ denote the final states for proton and alpha emission, respectively. The total intensity of particles with energy $E_x$ is then obtained by summing over all intermediate spins and parities and over all final states

$$I_x(E_x) = \sum_f \sum_i I_x^{if}(E_x) , \quad (4.6)$$

and the particle branching ratio $P_x$ by integration of this expression

$$P_x = \int_0^{E_x max} I_x(E_x)\, dE_x . \quad (4.7)$$

The input parameters in calculations of particle spectra are the initial and final spins and parities, the excitation energies of the final states, the $Q_\beta$ value, and the particle separation energies. Most of these parameters for the nuclei under consideration are not known experimentally and an analysis of the experimental delayed particle spectra with the statistical model might give us more information about them and also about the strength functions involved. The delayed particle data will probably offer the best possibility to get such information for nuclides very far from stability.

### 4.1 $Q_\beta$ values and particle separation energies

From the proton-511 keV gamma coincidence the $Q_\beta$-$B_p$ value for $^{116}$Cs was determined as 6.45 MeV[45,49]. The result of a calculation based on this value is shown in Fig. 9. The bell-shaped envelope of the spectrum is well reproduced. The steep increase of the intensity at the low-energy part is due to the strong influence of the Coulomb barrier on the proton widths while the decline towards higher energies reflects the beta intensity distribution. It is well known that the beta strength functions vary slowly with energy[12,14]; therefore the parameter $Q_\beta$-$B_p$ (or $Q_\beta$-$B_\alpha$) may under favourable circumstances be obtained from a precise fit to the high-energy part of the spectrum. In cases with good statistics and low background such an analysis can give good estimates of the end-point energy. Figure 10 shows the $^{120}$Cs delayed alpha spectrum[8] compared to calculations with different $Q_\beta$-$B_\alpha$. The best fit is obtained with the difference $Q_\beta$-$B_\alpha$ = 9.2 MeV. Figures 11 and 12 display the fits to the $^{118}$Cs data. With the value $B_\alpha$ = -1.5 MeV taken from the systematics[79] the $Q_\beta$ value is obtained from the delayed-alpha end-point

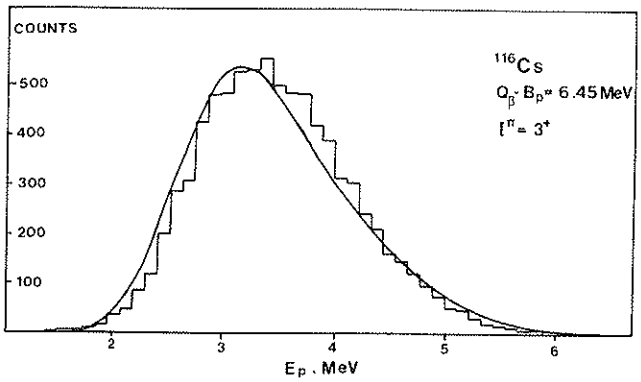


Fig. 9 The measured delayed-proton spectrum for $^{116}$Cs (histogram) compared with a calculation assuming $I^\pi = 3^+$ and a constant beta strength function. The experimental $Q_\beta - B_p$ value was used in this calculation. See also Table 3.

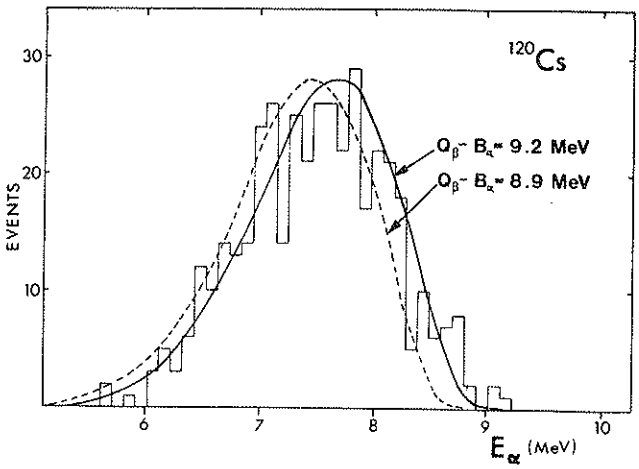


Fig. 10 The measured delayed-alpha spectrum from $^{120}$Cs (Ref. 8) compared with calculations assuming $Q_\beta - B_\alpha$ = 8.9 MeV and 9.2 MeV, respectively. The experimental value (Ref. 81) on the spin was used (I = 2) and the parity of $^{120}$Cs was assumed positive. The best fit is obtained with $Q_\beta - B_\alpha$ = 9.2 MeV. See also Table 3.

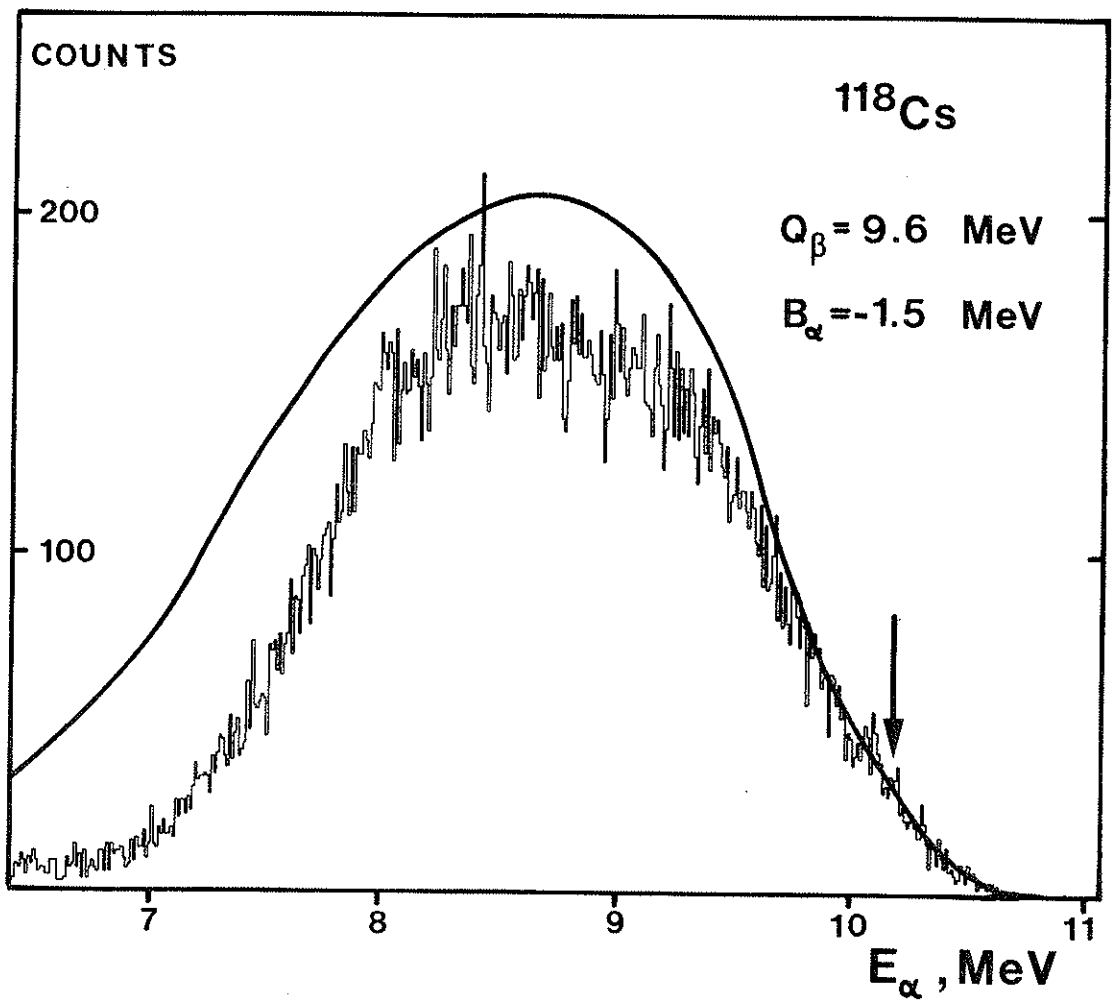


Fig. 11 Delayed alpha spectrum from $^{118}$Cs measured with a 100 μm, 150 mm$^2$ singles surface barrier detector. The experimental resolution was 20 keV FWHM. The end-point of the spectrum is fitted to a calculation assuming constant beta and alpha strength functions. The arrow indicates the normalization point.

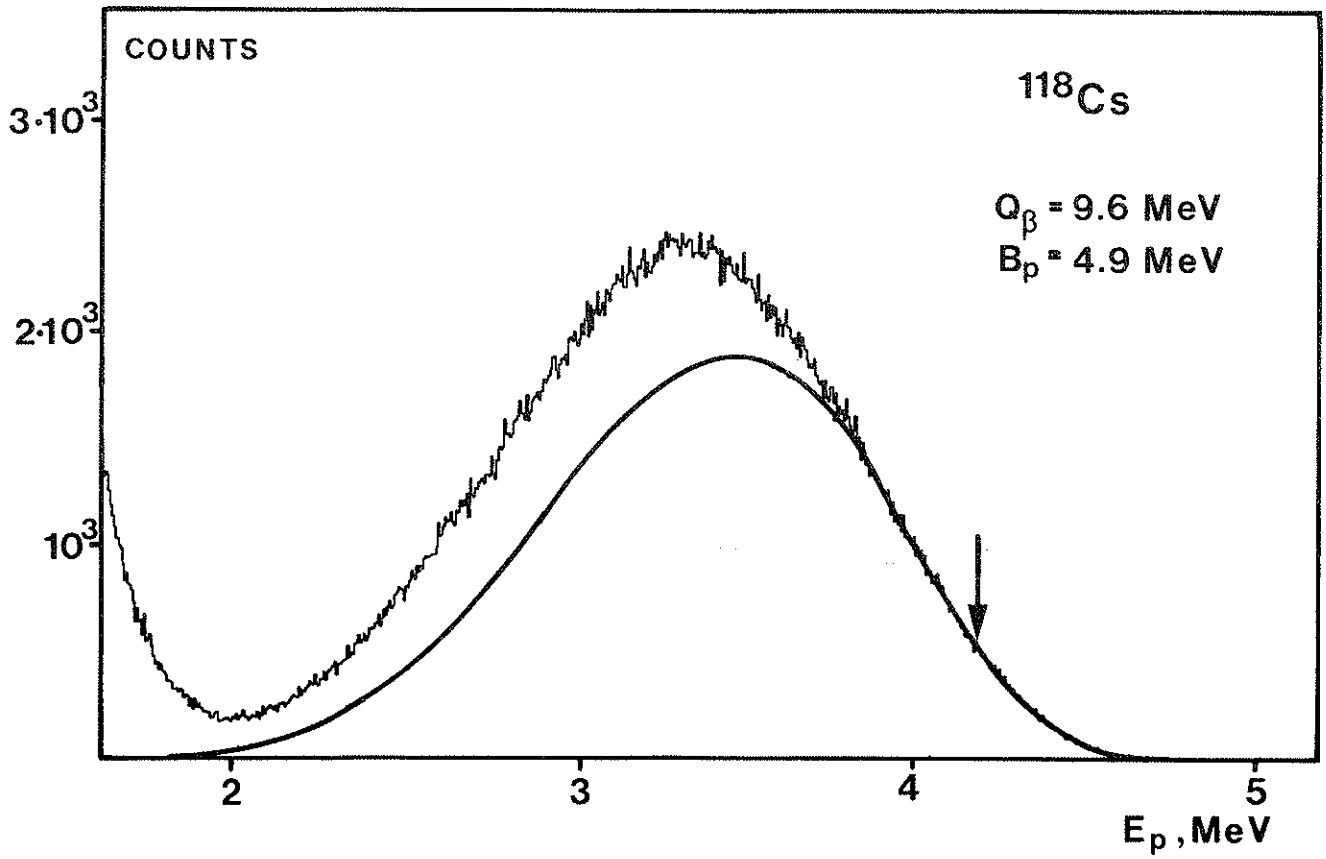


Fig. 12 Delayed proton spectrum for $^{118}$Cs. The spectrum was counted simultaneously with the alpha spectrum shown in Fig. 11. The experimental $Q_\beta - B_p$ value was used, and the $^{118}$Cs ground state spin-parity was assumed to be $I^\pi = 3^+$. The arrow indicates the normalization point.

Table 3

Calculations of branching ratios for delayed alpha emitters

| Nuclide | $Q_\beta$ (MeV) | $B_p$ (MeV) | $B_\alpha$ (MeV) | $I^\pi$ | $P_\alpha$(exp) | $P_\alpha$(calc) | $(P_p/P_\alpha)_{exp}$ | $(P_p/P_\alpha)_{calc}$ | $S_\alpha$ (MeV$^{-1}$) |
|---|---|---|---|---|---|---|---|---|---|
| $^{120}$Cs | 8.3 | 5.6 | -1.0 | $2^+$ | $(2.0\pm0.4)\times10^{-7}$ | $1.4\times10^{-7}$ | 0.36±0.10 | 0.26 | 0.02 |
| $^{118}$Cs | 9.6 | 4.9 | -1.5 | $3^+$ | $(2.4\pm0.4)\times10^{-5}$ | $3.9\times10^{-6}$ | 17.2±0.3 | 18.9 | 0.10 |
| $^{116}$Cs | 10.5 | 4.1 | -2.0 | $3^+$ | $(6\pm1)\times10^{-5}$ | $4.6\times10^{-5}$ | 51±5 | 50 | 0.02 |
| $^{114}$Cs | 12.0 | 3.3 | -2.8 | $3^+$ | a) | $1.0\times10^{-3}$ | 33±12 | 40 | - |
| $^{76}$Rb | 9.7 | 7.3 | 4.0 | $1^+$ | $(3.8\pm1.0)\times10^{-9}$ | $7.6\times10^{-9}$ | a) | | 0.01 |
| $^{181}$Hg | 7.46 | 1.31 | -5.76 | $\frac{1}{2}^-$ | $(1.2\pm0.4)\times10^{-7}$ | $6.0\times10^{-8}$ | $(1.5\pm0.6)\times10^3$ | $0.6\times10^3$ | 0.03 |

a) Not determined.

as 9.6 MeV, and the $B_p$ value is given by the experimental difference $Q_\beta$-$B_p$ (Ref. 7). Both the alpha and proton separation energies are expected to vary smoothly with mass number. If we assume that the trend follows the predictions given by the Myers and Swiatecki mass formula[80] and normalize to the $^{118}$Cs results, we arrive at the values for $Q_\beta$, $B_p$, and $B_\alpha$ given in Table 3. The calculated proton and alpha branches and their ratios are well reproduced with this set of parameters. The table also includes the results for $^{118}$Hg (Ref. 52) and $^{76}$Rb (Ref. 45).

### 4.2 Spins and parities

The calculated absolute intensities and relative feeding to final states are strongly dependent on the assumptions made about the initial and final spins and parities. This was discussed by Hornshøj et al.[60] who showed that the $^{115}$Xe delayed-proton gamma-coincidence data could be explained with the assumption $I_i^\pi = 5/2^+$ (Table 4). The rapid development of on-line measurements of spins with the ABMR and the optical pumping methods[81,82] will hopefully

Table 4

Calculation[a] of the relative and absolute proton intensities from $^{115}$Xe for various values of the initial spin and parity

| Assumed $I^\pi$ | Relative intensity (%) | | | Absolute intensity $P_p$ |
|---|---|---|---|---|
| | 0.0 MeV ($0^+$) | 0.71 MeV ($2^+$) | 1.48 MeV ($4^+$) | |
| $1/2^-$ | 92.3 | 7.7 | 0.0 | $9.6\times10^{-3}$ |
| $3/2^-$ | 79.7 | 20.0 | 0.3 | $5.6\times10^{-3}$ |
| $5/2^-$ | 62.4 | 36.0 | 1.6 | $2.8\times10^{-3}$ |
| $7/2^-$ | 2.1 | 87.8 | 9.8 | $7.0\times10^{-4}$ |
| $1/2^+$ | 83.5 | 16.4 | 0.0 | $9.6\times10^{-3}$ |
| $3/2^+$ | 72.8 | 27.1 | 0.1 | $6.4\times10^{-3}$ |
| $5/2^+$ | 41.1 | 55.7 | 3.2 | $2.3\times10^{-3}$ |
| $7/2^+$ | 33.2 | 56.3 | 10.5 | $1.1\times10^{-3}$ |
| Experiment[b] | ~ 40 | 58±7 | < 2 | $(3.6\pm0.6)\times10^{-3}$ |

a) $Q_\beta$ = 8.11 MeV, $B_p$ = 1.94 MeV.
b) Ref. 44.

provide us with experimental values for this parameter in many of the nuclides of interest here. Such information is of major importance for the interpretation of the particle data.

### 4.3 The beta strength functions

The high-energy beta decay originates mainly in the paired system of the nucleus, and a schematic model of the beta feeding with no strength below the energy corresponding to a hole-particle state has therefore been adopted in the calculations[60]. The experimental data[12,14] further suggest a slow variation in energy for the neutron-deficient nuclei, and the model strength function has been taken to be constant above the cut-off energy. The observed delayed-proton intensities are well reproduced with this model[7,60]. The gross theory of beta decay yields the best results until now for the delayed-neutron intensities[83], and it has also been shown[84] to give results in close agreement with previous calculations[7,60] for the delayed-proton intensities.

An analysis of the $^{115}$Xe delayed-proton spectrum[60] showed that the best agreement with the experimental spectral shape was obtained if the beta strength in the calculations was assumed to have the energy distribution according to the solid curve in Fig. 13. The peak in the strength was interpreted as a "pygmy" resonance originating in a $(g^p_{9/2})^{-1}g^n_{7/2}$ hole-particle excitation and should thus be a collective effect of the decay of the 10 protons in the $g_{9/2}$ proton shell to the $g_{7/2}$ neutron shell. Analyses of the $^{109}$Te (Ref. 35) and the $^{121,119}$Ba, $^{116}$Cs data[49] have indicated similar resonance structures, which is also supported by results from shell-model calculations including pairing corrections[85-87].

The proton width is a strongly increasing function of the excitation energy, and at the top of the excitation spectrum proton emission might become the dominating decay channel. The proton intensity is then a direct measure of the intensity of the beta feeding and the absolute strength might be determined, as has been shown for $^{115}$Xe (Ref. 14).

### 4.4 The proton strength functions

An extraction of the beta strength function from the delayed-proton data involves the assumption that the proton strength function is known or that the decay is dominated by one single proton channel. Neither of these assumptions is generally valid and

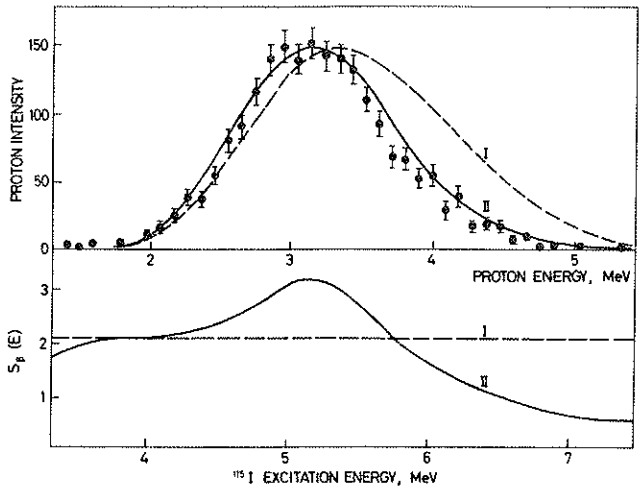


Fig. 13 The measured delayed-proton spectrum (upper graph) of $^{115}$Xe (exp. points) compared with two calculations (Ref. 60), both assuming $I^{\pi} = 5/2^+$. In one calculation the beta strength function is assumed constant, in the other it has been assumed to have the shape shown in the lower graph. The experimental (Ref. 44) $Q_\beta - B_p$ value was used in this calculation.

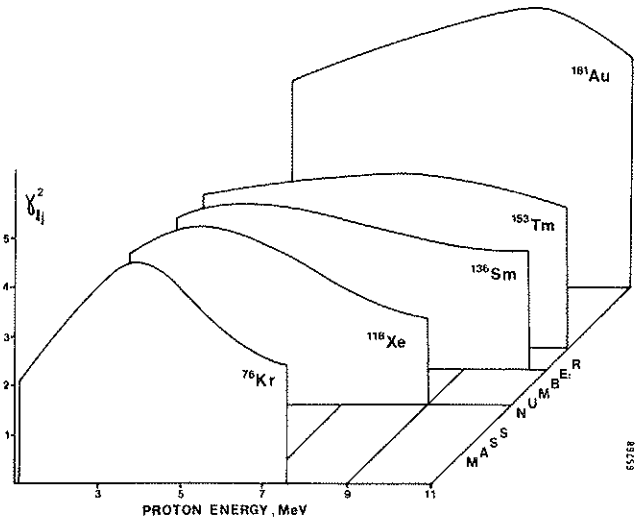


Fig. 14 The energy dependence of $\gamma^2_{\ell j}$ [Eq. (4.9)] calculated with the optical model parameters given in Ref. 89. The parameter $\gamma^2_{\ell j}$ is proportional to the proton strength function, which according to this calculation has a smooth dependence with the energy.

one has to be careful with the interpretations. Let us take a look at the proton strength functions used in the present calculations. The proton width is obtained from the expression

$$\Gamma_p^{if}(E_p) = \sum_{j\pi_i\pi_f} T_{\ell j}(E_p)/2\pi\rho_i(E) \qquad (4.8)$$

where $T_{\ell j}$ is the transmission coefficient calculated from the optical model potential and $\rho_i(E)$ the density of final levels with spin-parity $I_i^{\pi_i}$. The proton strength function $S_p$ is proportional to the quantity

$$\gamma^2_{\ell j} = T_{\ell j}/P_\ell \ , \qquad (4.9)$$

where $P_\ell$ is the WKB penetrability[88]. The behaviour of $\gamma^2_{\ell j}$ as a function of energy, calculated with the optical model parameters given in Ref. 89, is shown in Fig. 14 for $s_{1/2}$ proton waves. This figure serves as an illustration of the smooth energy behaviour of $S_p$ used in the present calculations. We have, however, to point out that we have not yet sufficient experimental knowledge about the proper optical model parameters at low kinetic energies and low binding energies to make any precise predictions. The delayed proton data might here play an essential role in a further understanding of the sub-barrier penetrabilities.

### 4.5 The alpha strength functions

The $^{181}$Hg delayed-alpha intensity[52] was used to give an estimate of the cluster strength function ($^{177}$Ir + α) in $^{181}$Au at 4-6 MeV excitation energies. In terms of the Wigner limit[90] the $^{181}$Au ground state width $\theta^2_{\alpha,g}$ is 0.006 and the cluster strength was found to be 0.02 MeV$^{-1}$ at 4-6 MeV. The quantity $S_\alpha/\theta^2_{\alpha,g}$ is thus ∿ 3 MeV$^{-1}$. This value is of the same order of magnitude as the estimate[91] of 0.1-1 MeV$^{-1}$ at 5-10 MeV excitation in the rare-earth region obtained from the data on alpha emission from resonances populated in slow neutron reactions[92].

In the present calculations, we have assumed the alpha strength to correspond to the Wigner limit ($\gamma^2_W = 3\hbar^2/2M_r a^2$) divided by the cluster level spacing, which is twice the distance between the harmonic oscillator levels:

$$S_\alpha = \frac{\gamma^2_W}{2\hbar\omega} \ . \qquad (4.10)$$

The channel radius a is taken as 1.55 $A^{1/3}$ fm, and $M_r$ denotes the reduced mass of the alpha particle. The experimental width can be expressed[10] as

$$\Gamma_\alpha = 2P_\ell\gamma^2 \ , \qquad (4.11)$$

and with $S_\alpha = \gamma^2\rho$ we get the expression for the alpha width as

$$\Gamma_\alpha = \frac{\gamma^2_W P_\ell}{\hbar\omega\rho} \ . \qquad (4.12)$$

The penetrability $P_\ell$ was calculated with the diffuse surface potential[93] used by Rasmussen[94]. The results of calculations, with the assumption of a constant alpha strength function over the excitation region of interest, given in Table 3, show that Eq. (4.10) gives a rather good estimate of the alpha strength function. The last column in the table gives the alpha strength obtained from a normalization of the calculated to experimental intensity.

## 5. Fluctuation phenomena

The structure of the resonances populated in the high-energy beta decay is complex, and we have seen that a statistical approach is quite reasonable as a first approximation. The fine structure observed in the high resolution measurements of delayed particle spectra gives us a first indication of the microscopic structure involved. In the medium-weight and heavy-mass regions the average level distances are generally much smaller than the resolution of the spectrometers available and we cannot

resolve each single state. In such unresolved spectra we observe fluctuations in the intensity due to the wide distributions of the quantities involved[22]. We may then again adopt the statistical theory which, besides the average properties, is capable of making predictions about the expected fluctuations around the average. The individual parameters (spacings, widths) are then considered as stochastic variables and the experimental spectrum represents a "sample" of this variable. Each single state has, of course, its own specific properties, and a given nucleus will therefore always represent the same sample. It is not permissible in the statistical approach to ask whether a certain peak is real. It is! The question is, however, whether it possesses properties that cannot be understood from the statistical model alone, so that it must be assigned quantum numbers other than spin and parity.

Let us first consider some simple distribution functions that are relevant to the delayed-particle spectra, and discuss their consequences for the interpretation of the experimental results.

## 5.1 Fluctuations in the level distances

The average level distances decrease dramatically with energy. The level-to-level distances of states with a given spin and parity fluctuate around an average value, and it has been found that the distribution obeys the Wigner law[95a]. The probability of finding the next level away from a given one in an interval (D, D + dD) is, according to this law,

$$p(D)\,dD = \frac{\pi D}{2\langle D\rangle^2}\exp\left[-\frac{\pi D^2}{4\langle D\rangle^2}\right]dD\,, \qquad (5.1)$$

where $\langle D\rangle$ denotes the mean spacing. This narrow distribution, with the normalized variance, $\mathrm{Var}\,(D/\langle D\rangle) = 0.27$, has a vanishing probability of zero spacing between levels. If the distances in a given excitation region were statistically independent, the $n^{th}$ order spacing would have a normalized variance of $0.27/n$; however, long-range correlations[95b] give an even faster decrease with n. The fluctuations in the level distance may therefore be neglected in all cases where the experimental resolution includes a few resonances on the average.

## 5.2 Fluctuations in the level widths

A much more important fluctuation effect is found for the transition widths $\Gamma_f$ to a single final state f. Such fluctuations are described by the Porter-Thomas law (PT)[96] which is appropriate to one single channel and non-overlapping levels. The frequency distribution is*)

$$p(\Gamma_f) = \left[\frac{1}{2\pi\langle\Gamma_f\rangle\Gamma_f}\right]^{\frac{1}{2}}\exp\left[-\frac{\Gamma_f}{2\langle\Gamma_f\rangle}\right], \qquad (5.2)$$

where $\langle\Gamma_f\rangle$ is the mean value. The PT distribution is very skew with $\mathrm{Var}\,(\Gamma_f/\langle\Gamma_f\rangle) = 2$, which means that there are many small values (the most probable one is zero) and a few large ones. The reduced beta transition probability and the particle decay widths to a final level are expected to be governed by this law. In a delayed particle spectrum with only one dominating outgoing particle channel, the fine structure in the spectrum is due to PT fluctuations of the individual beta transitions. Examples of this may be found, for example, in some of the delayed neutron spectra[64-67].

The total gamma width may be assumed to be constant because of the many partial gamma widths which contribute to the total width[95c]. In a delayed particle spectrum where the total width is dominated by the (non-fluctuating) gamma width, the distribution is governed by the product of the beta intensity and the partial particle widths, which are both PT-distributed. If we let x and y denote two PT distributions (with $\langle x\rangle = \langle y\rangle = 1$), the observed intensity is $v = x\cdot y$, which has the probability density[13,97]

$$p(v) = K_0(v^{\frac{1}{2}})/\pi v^{\frac{1}{2}}\,, \qquad (5.3)$$

where $K_0$ denotes the modified Bessel function. To illustrate the outcome of an experiment where such a distribution function governs the decay, Fig. 15 shows a simulated set of product-distributed intensities folded with a Gaussian function which represents the detector response function. Strong fluctuations are observed, bot one notes that the number of "peaks" is much smaller than the actual number of levels involved. An interpretation of an experimental spectrum of this type should therefore necessarily take into account the contribution from the unresolved (weak) transitions.

The distribution corresponding to the ratio of two PT-distributed variables, $z = x/y$, has the frequency function

$$p(z) = \frac{1}{\pi z^{\frac{1}{2}}(z+1)}\,. \qquad (5.4)$$

This function is normalized but has no higher moments. An example of the consequences of this function was recently pointed out in the interpretation of the results from the $^{84}Rb(n_{th},p)^{84}Kr$ reaction[98]. The relative proton intensity to the $0^+$ and $2^+$ states in $^{74}Kr$ was found to be $\Gamma_p(0^+)/\Gamma_p(2^+) = 4.7 \pm 0.7$. A statistical model calculation predicted this ratio as 7.9 and 0.36, for the spin $3/2^-$ and $5/2^-$ of the capture state, respectively. The interpretation has, however, to be made with some care since the calculation represents the average over many levels, while the experiment measures the ratio of two individual widths. With the distribution function according to Eq. (5.4), we find a 17% probability for a $5/2^-$ state to give a value greater than or equal to the one obtained experimentally. The fluctuation effect obviously rules out the possibility of making a safe spin assignment in this case. Another example, where this distribution might be of importance, is given by the experimental observation of weak gamma-rays to the ground state in competition with a strong neutron channel[99-101] ($\Gamma_{\gamma 0} \ll \Gamma_n$). The individual gamma transition probabilities are assumed to be PT-distributed.

A slightly more complicated function is

$$z = \frac{x}{x + ay} \qquad (5.5)$$

in which the constant a denotes the ratio between the two widths. The frequency function for this expression is

$$p_1(z) = \frac{a^{\frac{1}{2}}}{\pi(1-z)^{\frac{1}{2}}z^{\frac{1}{2}}[1 + (a-1)z]}\,, \qquad (5.6)$$

*) This function is a chi-square distribution with one degree of freedom.

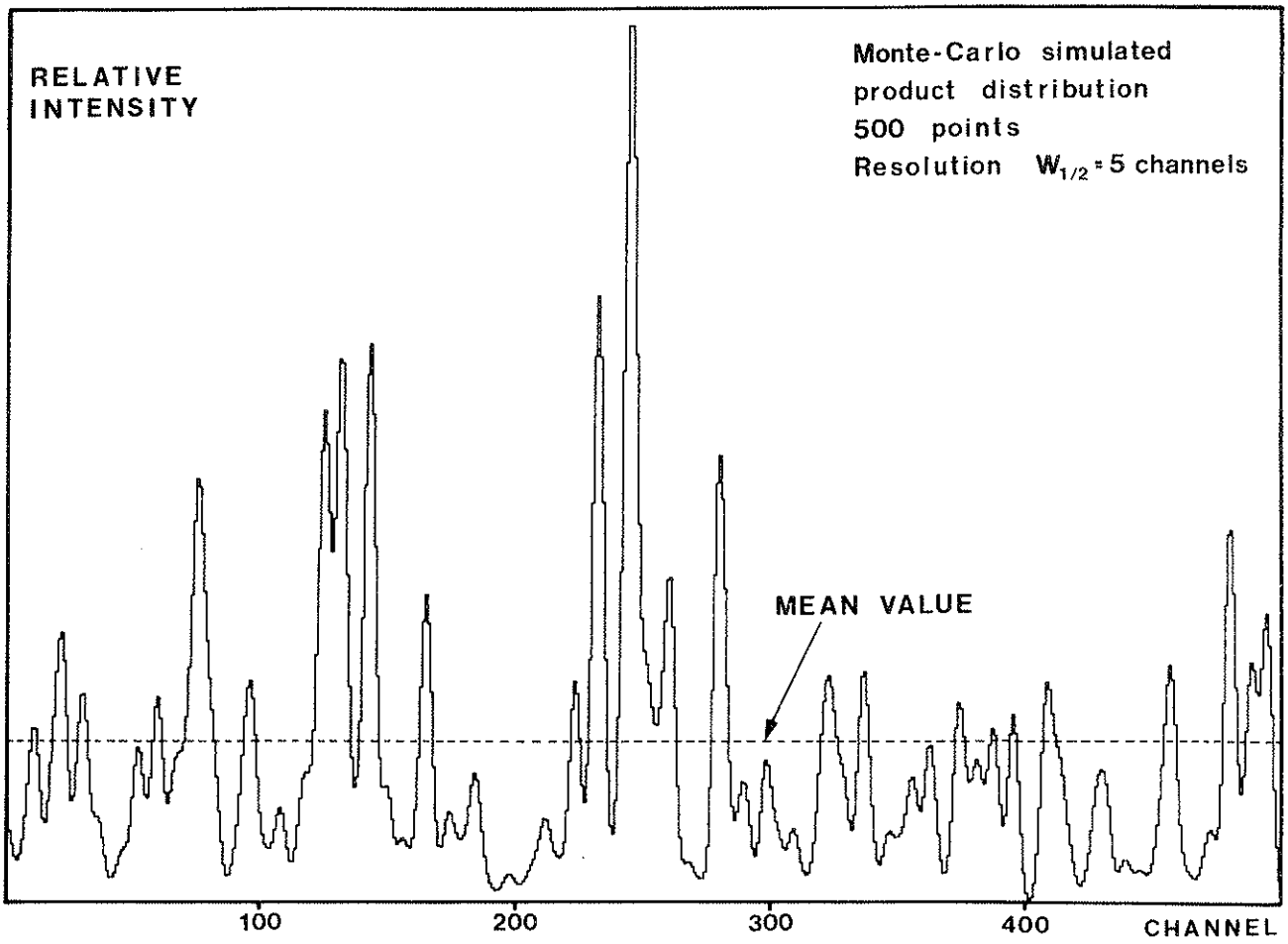


Fig. 15 A sequence of 500 equally spaced random numbers of the product distribution [Eq. (5.3)] sampled by a Monte-Carlo technique and smoothed with a Gaussian function (half-width 5 channels).

with

$$\langle z \rangle = (1 + \sqrt{a})^{-1} \qquad (5.7)$$

and

$$\mathrm{Var}\ z = \frac{\sqrt{a}}{2(1 + \sqrt{a})^2} \, . \qquad (5.8)$$

The most striking property of this distribution is the strong enhancement of a relatively weaker branch in a case in which we are concerned with two PT variables. If, as an example, the intermediate nucleus in a delayed particle process has two outgoing channels, with one $10^4$ times stronger than the other, the experiment would still show a 1% branch for the weaker component.

The theoretical expression of a compound nucleus with competing particle and gamma channels can be written in a simplified form as

$$z = \frac{x}{x + ay + b} \, , \qquad (5.9)$$

in which the constant b represents the total (non-fluctuating) gamma width. This expression has a complicated frequency function[97] and the distribution is best handled, as in the general case, by numerical methods. A useful quantity in these investigations is the *fluctuation function* S, defined as[102]

$$\langle f(x,y,\ldots,a,b) \rangle = S(a,b)\ f(1,1,\ldots,a,b) \, . \qquad (5.10)$$

This function is in most cases close to one, but in some cases dramatic deviations occur. The fluctuation function for Eq. (5.9) is displayed in Fig. 16 for different values of a and as a function of b. For large values of b, S is unity, while as b approaches zero, we have $S(a) = (1 + a)/(1 + a^{\frac{1}{2}})$. In many practical cases the strongest particle channel is of the same order as or greater than the total gamma width over a large part of the spectrum, and, as shown in Fig. 16, the fluctuation correction then becomes important for a correct interpretation. An example would be a delayed alpha spectrum where the high-energy part becomes enhanced owing to this effect. [The gamma width, represented by b in Eq. (5.9) becomes smaller than the strongest particle channel in the upper part of the spectrum.] This will then give a significant spectral distortion compared to the shape expected from the statistical model, as discussed in Section 4.

A function that closely resembles the compound nucleus expression [Eq. (4.3)] is obtained if Eq. (5.9) is multiplied with another PT-distributed variable w. It is trivial to show that the new function, $u = w \cdot v$, has the same fluctuation function as the one displayed in Fig. 16.

Let us finally investigate how the fluctuations in the level widths may influence lifetime measurements of excited states in the compound nucleus

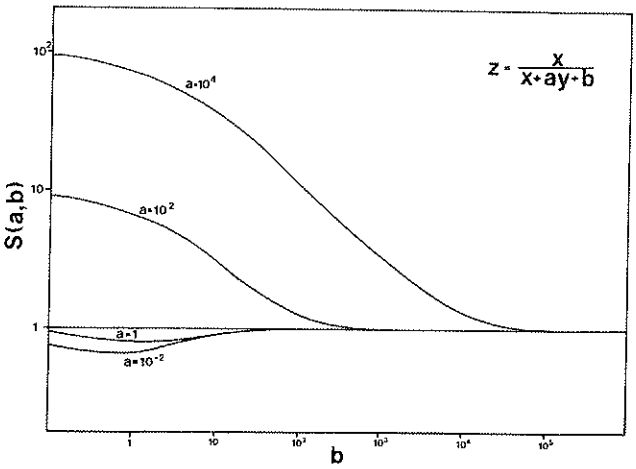


Fig. 16 The fluctuation function for the expression x/(x + ay + b) for different values of the parameter a and as a function of b. With b = 0 the fluctuation function becomes $S(a) = (1 + a)/(1 + \sqrt{a})$.

region. If we neglect the way in which the resonances were formed and observe their decay through the weak channel x (with the width $\Gamma_x$) with a competing decay channel y ($\Gamma_y$) we get the probability for the decay of one single state as

$$P_x(t) = \frac{\Gamma_x}{\hbar} e^{-[(\Gamma_x+\Gamma_y)t]/\hbar} . \qquad (5.11)$$

The average decay of the channel x would then intuitively follow an exponential decay law. If, however, the two variables x and y are PT-distributed, we find a different relation for the decay law[97], namely

$$P_x(t) = \frac{\langle\Gamma_x\rangle}{4\hbar} \frac{1}{\left(\frac{\langle\Gamma_x\rangle}{\hbar}t + \frac{1}{2}\right)^{3/2}\left(\frac{\langle\Gamma_y\rangle}{\hbar}t + \frac{1}{2}\right)^{1/2}} , \qquad (5.12)$$

which gives a $t^{-2}$ behaviour for large values of t. An example, where these corrections may be of importance, is found in the lifetime measurements of highly excited states from the delayed proton-KX-ray measurements[105].

A summary of some of the properties of a number of simplified distribution functions is given in Table 5 [103,104].

## 5.3 The analysis of unresolved delayed-particle spectra

The experimental line width in the delayed-particle spectra discussed in this paper is of the same order as or greater than the average level spacing. The fine structure observed then represents gross fluctuations of the type first discussed by Egelstaff[22]. The simulated spectrum in Fig. 15 illustrates this effect. It would be interesting if one could get information on the intermediate structure, but in most cases the experimental resolution does not allow this. The fluctuations provide us, however, with an experimental tool for measuring level densities of nuclei far from beta stability. An outline of such an analysis is given in the following[97].

5.3.1 Theoretical estimate of Var $(I_x/\langle I_x\rangle)$. A theoretical expression for the variance in a delayed particle spectrum, where the detector half-width $W_{\frac{1}{2}}$ is much greater than the average level spacing, has been given by Hansen[106]. The intensity of one individual line (which in the experimental case is unresolved) in the particle spectrum is

$$R_x^{if\nu} = R_\beta^{i\nu} \frac{\Gamma_x^{if\nu}}{\Gamma_{tot}^{i\nu}} \qquad (5.13)$$

in which $R_\beta^{i\nu}$ is the beta feed to the $\nu^{th}$ resonance with spin and parity $I_i^{\pi i}$. The normalized variance for this quantity

$$(R_x^{if})^{-2} \text{ Var } R_x^{if} \equiv \alpha^{if} \qquad (5.14)$$

is relatively complicated[106,107] and we shall only consider the two limiting cases here. If $\Gamma_x^{if\nu} = \Gamma_{tot}^{i\nu}$ the variance is only due to the fluctuations in the beta intensity (which is PT-distributed) and we get $\alpha^{if} = 2$. In a case where the total width $\Gamma_{tot}^{i\nu}$ is dominated by the gamma width, the value becomes instead $\alpha^{if} = 8$ [the distribution function is the product law Eq. (5.3)].

The variance in the total particle intensity [Eq. (4.6)] can then be obtained by weighting the individual contributions [Eq. (5.14)] according to the detector response function (here represented by a Gaussian) and by summing over all intermediate spins and all final states

$$\text{Var } I_x = (2 \ln 2)^{\frac{1}{2}}\pi^{-\frac{1}{2}}W^{-1}\sum_f \sum_i \left(I_x^{if}\right)^2 D_i\alpha^{if} . \qquad (5.15)$$

The variance, Var $(I_x/\langle I_x\rangle) = \langle I_x\rangle^{-2}$ Var $I_x$, calculated from this expression may then be compared with the experimental variance. Since the detector resolution is known, such a comparison gives a measure of the average level spacing, $D_i$, at the actual excitation energies.

5.3.2 The variance from the measured spectra. The experimental spectra from $^{115}$Xe and $^{111}$Te have been analysed[7,107] and the variance was calculated for different parts of the spectrum. The main trend of the variance followed the predictions from Eq. (5.15).

Let us here outline a more convenient method of analysis based on the autocorrelation functions for the spectra. Consider first the case of one intermediate spin only, an assumed constant level spacing D, and a detector characterized by a Gaussian resolution parameter $\sigma(\gg D)$. Let the spectrum have unit average intensity $\langle g(x)\rangle = 1$ with the normalized variance $\alpha$ for the individual line. One then finds for the autocorrelation function

$$\psi_g(\tau) = \langle g(x)g(x+\tau)\rangle = 1 + \frac{\alpha D}{2\pi^{\frac{1}{2}}\sigma} \exp\left(-\frac{\tau^2}{4\sigma^2}\right) . \qquad (5.16)$$

Note that this expression in principle permits the determination not only of the combination $\alpha D/\sigma$ but also of the experimental resolution. A corollary is that one may use the method of Rice[108] to predict the number of maxima $n_M$ per unit energy

$$n_M = \frac{1}{2\pi}\left(\frac{3}{2}\right)^{\frac{1}{2}}\frac{1}{\sigma} = \frac{0.456}{W_{\frac{1}{2}}} , \qquad (5.17)$$

where $W_{\frac{1}{2}}$ is the FWHM of the resolution function. The simulated spectrum given in Fig. 15 provides one example of this relationship; the density of maxima is 41/500 = 0.080 channel$^{-1}$, where the predicted value according to Eq. (5.17) is 0.456/5 = 0.091 channel$^{-1}$.

The theory refers to a "true average" of the spectrum. As this is unknown, a method was developed[7,106] where one analysed a new spectrum obtained from the difference between the measured one and one smoothes with a Gaussian function giving the effective resolution $\sigma_>$. The variance calculated

Table 5 [a]

Mean values and fluctuation functions for some simplified distributions

| f | ⟨f⟩ | S(a,b) | Comments, references |
|---|---|---|---|
| $x$ | 1 | 1 | PT distribution, Var (f/⟨f⟩) = 2. Fluctuations in delayed particle spectra, weak gamma channel. |
| $\frac{xy}{b}$ | $\frac{1}{b}$ | 1 | Product distribution [Eq. (5.3)], Var (f/⟨f⟩) = 8. Fluctuations in delayed particle spectra, strong gamma channel. |
| $\frac{x}{ay}$ | Not defined | - | Proton emission from resonances populated in thermal neutron reactions, high-energy gamma-rays in competition with delayed neutrons. |
| $\frac{bx}{x+b}$ | $b\left\{1 - \left(\frac{\pi b}{2}\right)^{\frac{1}{2}} e^{b/2} \times \left[1 - \phi\left(\sqrt{\frac{b}{2}}\right)\right]\right\}$ | $(1+b)\left\{1 - \left(\frac{\pi b}{2}\right)^{2} \times \times e^{b/2}\left[1 - \phi\left(\sqrt{\frac{b}{2}}\right)\right]\right\}$ | Fluctuations in (n,γ) cross-sections, Ref. 95d. |
| $\frac{x}{x+ay}$ | $\frac{1}{1+\sqrt{a}}$ | $\frac{1+a}{1+\sqrt{a}}$ | Corrections to the observed intensity of the weaker component when the decay is a competition between two PT-distributed variables. Var (f/⟨f⟩) = 1/2 $a^{1/2}$. |
| $\frac{wx}{x+ay}$ | $\frac{1}{1+\sqrt{a}}$ | $\frac{1+a}{1+\sqrt{a}}$ | Var (f/⟨f⟩) = 2 + 3/2 $\sqrt{a}$ |
| $\frac{x}{x+ay+b}$ $\frac{wx}{x+ay+b}$ | No simple expression for ⟨f⟩ exists | Fig. 16 | Compare with the compound nucleus expression for delayed particle emission. |
| $\frac{x^2}{x+ay}$ | $\frac{2\sqrt{a}+1}{(\sqrt{a}+1)^2}$ | $\frac{(1+a)(2\sqrt{a}+1)}{(\sqrt{a}+1)^2}$ | Ref. 103 |
| $\frac{xy}{x+ay}$ | $\frac{1}{(\sqrt{a}+1)^2}$ | $\frac{1+a}{(1+\sqrt{a})^2}$ | Correction varies between 0.5 and 1. Ref. 104. |

a) x, y, and w are normalized PT variables with ⟨x⟩ = ⟨y⟩ = ⟨w⟩ ≡ 1.
a is a scale factor by which the channel y is faster than channel x.
b denotes the constant gamma width.

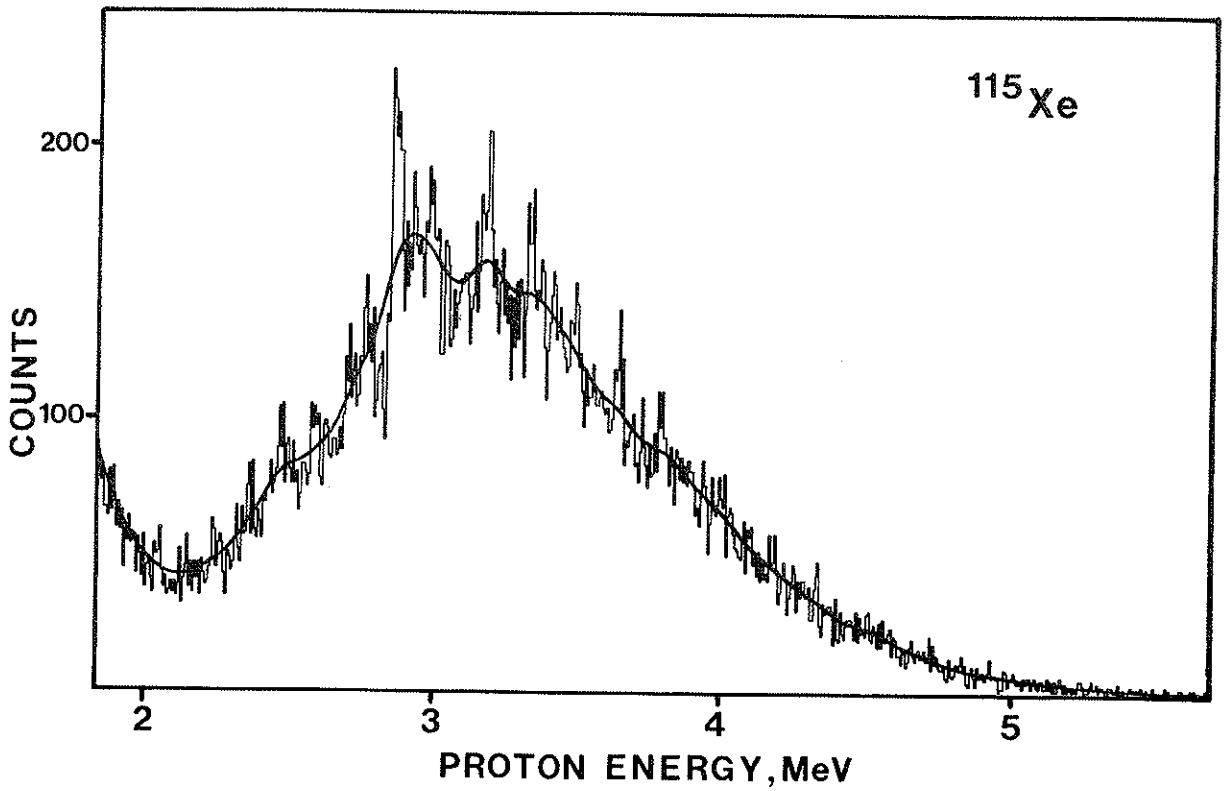


Fig. 17 The spectrum of beta-delayed protons from $^{115}$Xe determined with a 300 μm, 300 mm$^2$ singles surface barrier silicium detector. The energy resolution is around 15 keV for the protons. The curve shows the same spectrum smoothed with a Gaussian function having a half-width of 20 channels.

with this method is smaller than the real value by a factor

$$1 + \frac{1}{y} - \sqrt{\frac{8}{1+y^2}}\,, \qquad (5.18)$$

where $y = \sigma_>/\sigma$.

In the present analysis we also perform a smoothing of the measured spectrum, as illustrated in Fig. 17 for $^{115}$Xe. The new quantity

$$d(x) = g(x)/g_>(x) \qquad (5.19)$$

is then formed. The autocorrelation function for $d(x)$, $\psi_d(\tau)$, takes to a good approximation the form[97]

$$\psi_d(\tau) = 1 + \frac{\alpha D}{2\pi^2\sigma} \times$$

$$\times\left[ e^{-\frac{\tau^2}{4\sigma^2}} + \frac{e^{-\frac{\tau^2}{4\sigma^2 y^2}}}{y} - \frac{2\sqrt{2}}{\sqrt{y^2+1}}\, e^{-\frac{\tau^2}{2\sigma^2(1+y^2)}} \right]. \qquad (5.20)$$

Figure 18 shows the resulting autocorrelation function for $^{115}$Xe compared to the expression (5.20). From this one derives the experimental variance $\mathrm{Var}\,(I/\langle I\rangle)_{exp} = 0.021$ at 3.15 MeV proton energy, corresponding to about 5.2 MeV excitation energy in $^{115}$I. An analysis of the $^{111}$Te spectrum[26] is shown in Fig. 19. We may now proceed and compare the experimental values on the variance with those calculated from the Eq. (5.15). In this analysis we use the Fermi gas expression for the level density[109a]:

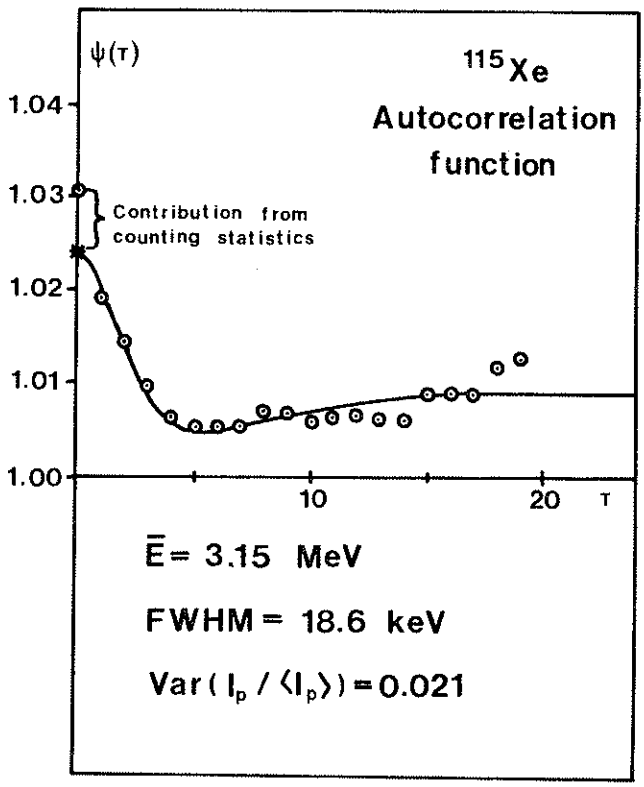


Fig. 18 The autocorrelation function for the $^{115}$Xe delayed proton spectrum shown in Fig. 17. The solid curve shows the theoretical curve [Eq. (5.20)].

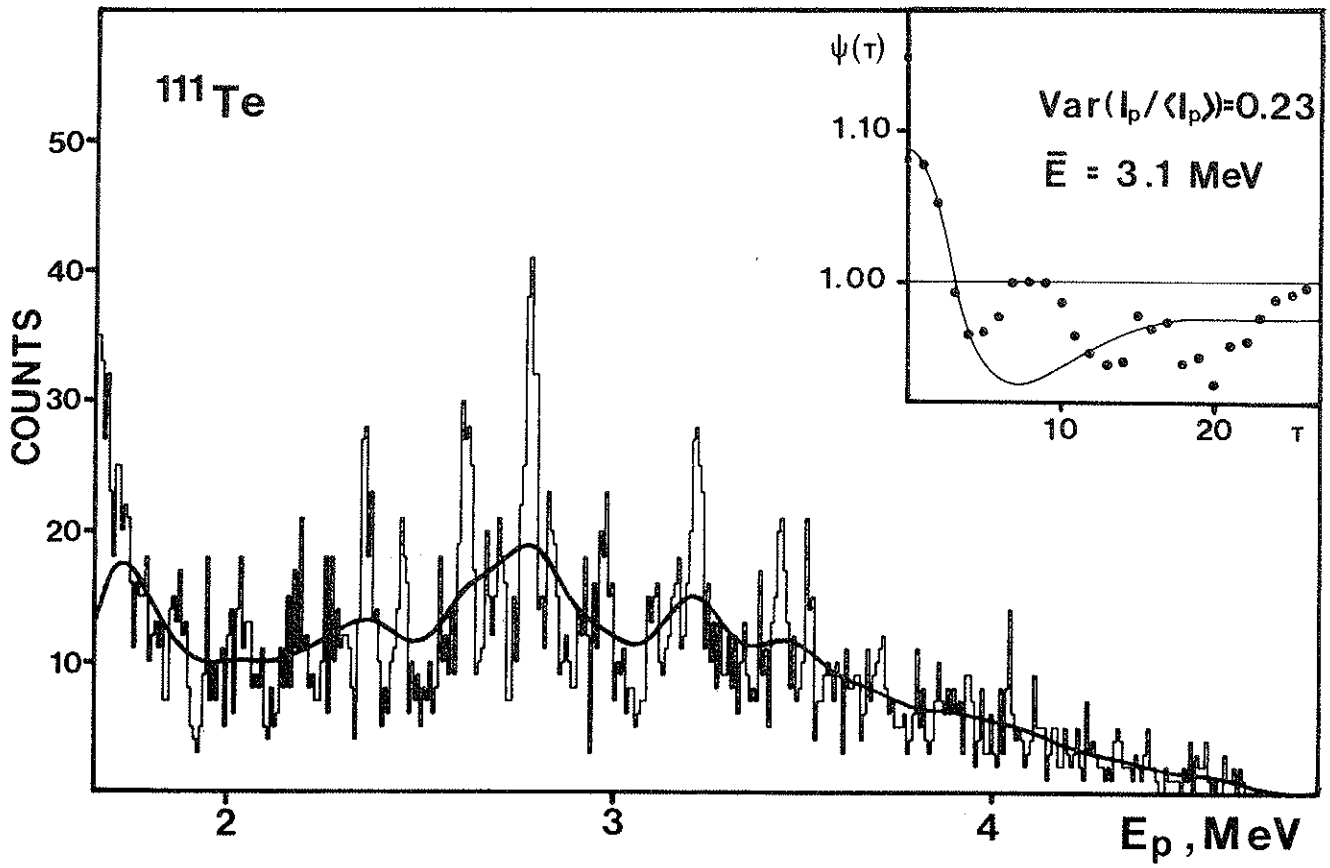


Fig. 19 Energy spectrum and autocorrelation function for $^{111}$Te (see captions to Figs. 17 and 18). The analysis indicates a detector resolution of 38 keV in this experiment, which is in agreement with the value of 30-40 keV given in Ref. 26.

$$\rho(E,I_i) = \frac{2I_i+1}{24}\sqrt{a}\left(\frac{\hbar^2}{2J_{rig}}\right)^{3/2}\frac{e^{2\sqrt{aU}}}{U^2} \qquad (5.21)$$

with

$$U = E' - (\hbar^2/2J_{rig})\, I_i(I_i+1)\ ,$$

where E′ is the effective excitation[109b], and with

$$\hbar^2/2J_{rig} = 26.7/A^{5/3}\ \text{MeV}\ .$$

The parameter a in Eq. (5.21) may now be fitted to the experimental data. Figure 20 shows the resulting a values as a function of the neutron number. The experimental points for $^{122,124}$Sb and $^{126,130}$I, where the average level density was taken from slow neutron data[110], are included. The lines show the A/8 behaviour which is known[109b] to follow the general trend of the Fermi gas level density parameter. The two curves show the behaviour of a according to the expression

$$a = A[0.139 + 0.0102\ (S-0.33D)] \qquad (5.22)$$

used in the level density formula by Gilbert and Cameron[4,5]. In Eq. (5.22) S denotes the total shell energy and D the "distance" to the nearest closed neutron or proton shell. The experimental data give level densities that are higher than the theoretical predictions and the shell effects are less pronounced than expected.

## 6. Concluding remarks

At this point it only remains to sum up what we have learned until now from the study of delayed particle emission, and to point very briefly to the prospects for further developments. In addition to the reassuring knowledge that the phenomenon semi-quantitatively may be understood in the framework of a compound-nucleus picture of nuclear beta decay, we have over the past years gained specific information on the following points:

1) Extension of the nuclear mass systematics from measured $Q_\beta$-B values.

2) Experimental demonstration of the very different energy dependence of $\beta^+$ and $\beta^-$ strength functions. This is taken as indirect evidence of the giant-resonance processes, which dominate the beta-decay rates.

3) Measurements of nuclear level densities away from stability via fluctuation analysis of the fine structure in particle spectra.

4) Fluctuation corrections to the spectral intensities -- in particular for the cases in which only few exit channels are open.

5) Estimates of the alpha-emission strength function at intermediate excitation energies. (From the intensities of beta-delayed alphas.)

To this list should be added the new results reported at this conference by Hardy:

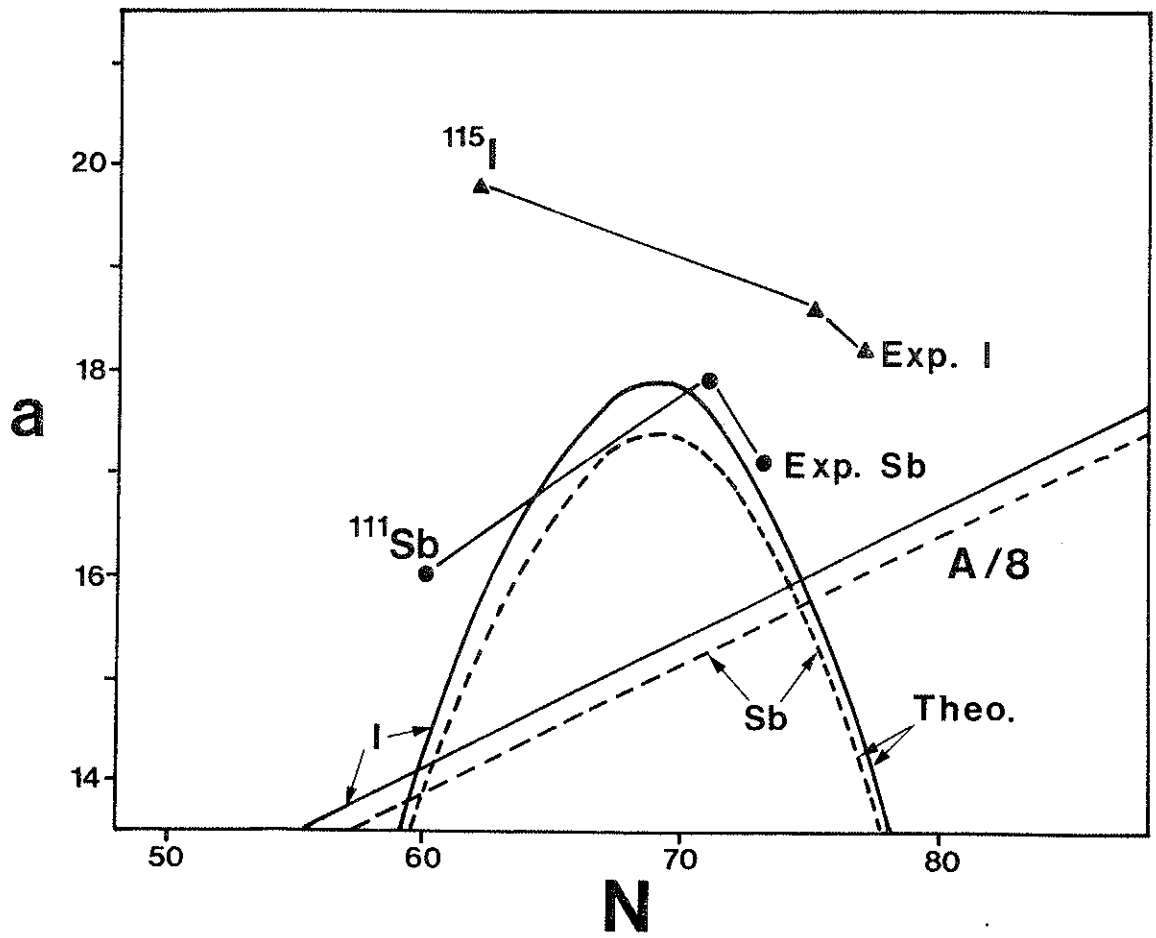


Fig. 20 The parameter a in the Fermi gas level density formula determined from an analysis of delayed proton spectra. The values for $^{122,124}$Sb, and $^{128,130}$I calculated from the average level spacings given in Ref. 110 are also included. The curves show the predicted behaviour of a according to Refs. 4 and 5.

6) Lifetimes of proton-emitting levels determined through p-KX coincidences.

Experimentally the basic parameters (spins, Q-values, beta strength function, optical-model assumptions, etc.) are, however, in most cases tied together in a way that makes their extraction difficult without very complete experimental information. As just one example one may imagine combining the measured proton widths (6) with a measured level density (3) in order to obtain a direct check on the proton strength predicted by the optical model for a very special situation: a low-energy proton with almost no binding in the nucleus.

The emission of delayed particles is *the* process characteristic of far-unstable nuclei; it is worth some effort to learn to make full use of it.

Acknowledgements

The authors are grateful to Drs. J.M. D'Auria and O.B. Nielsen for valuable comments on this paper.

References

1) H.L. Ravn, These proceedings.

2) Nuclear Data Sheets 17, 1 (1976).

3) A. Charvet, J. D'Auria, J. Genevey-Rivier, A. Huck, G. Klotz, A. Knipper, G. Marguier, C. Richard-Serre and G. Walter, These proceedings.

4) A. Gilbert and A.G.W. Cameron, Can. J. Phys. 43, 1446 (1966).

5) J.W. Truran, A.G.W. Cameron and E. Hilf, Proc. Internat. Conf. on the Properties of Nuclei far from the Region of Beta Stability, Leysin, 1970 (CERN 70-30, 1970), Vol. 1, p. 275.

6) H.L. Ravn, S. Sundell and L. Westgaard, Phys. Letters 39B, 337 (1972).

7) B. Jonson, Beta-delayed proton emission from isotopes of mercury, cesium, xenon and krypton, Thesis, Chalmers Univ. of Technology, Göteborg, Sweden, 1972.

8) P. Hornshøj, P. Tidemand-Petersson, R. Bethoux, A.A. Caretto, J.W. Grüter, P.G. Hansen, B. Jonson, E. Hagberg and S. Mattsson, Phys. Letters 57B, 147 (1975).

9) E. Hagberg, P.G. Hansen, P. Hornshøj, B. Jonson and P. Tidemand-Petersson, Abstract, Cargèse, 1976.

10) E. Vogt, Advances in Nuclear Phys. 1, 261 (1968).

11) A.M. Lane, R.G. Thomas and E.P. Wigner, Phys. Rev. 98, 693 (1955).

12) C.L. Duke, P.G. Hansen, O.B. Nielsen and G. Rudstam, Nuclear Phys. A151, 609 (1970).

13) P.G. Hansen, Advances in Nuclear Phys. 7, 159 (1973).

14) P. Hornshøj, B.R. Erdal, P.G. Hansen, B. Jonson, K. Aleklett and G. Nyman, Nuclear Phys. A239, 15 (1975).

15) K.H. Johansen, K. Bonde Nielsen and G. Rudstam, Nuclear Phys. A203, 481 (1973).

16) K. Aleklett, G. Nyman and G. Rudstam, Nuclear Phys. A246, 425 (1975).

17) M. Yamada, Bull. Sci. Eng. Research Lab. (Waseda University) No. 31-32 (1965).

18) K. Takahashi and M. Yamada, Progr. Theor. Phys. 41, 1470 (1969).

19) K. Takahashi, Progr. Theor. Phys. 45, 1466 (1971).

20) T. Kodama and K. Takahashi, Nuclear Phys. A239, 489 (1975).

21) G.A. Bartholomew, E.D. Earle, A.J. Ferguson, J.W. Knowles and M.A. Lone, Advances in Nuclear Phys. 7, 229 (1973).

22) P.A. Egelstaff, Proc. Phys. Soc. 71, 910 (1958).

23) V.A. Karnaukhov, G.M. Ter-Akopyan, L.A. Petrov and V.G. Subbotin, Soviet J. Nuclear Phys. 1, 581 (1965).

24) A.T. Siivola, Phys. Rev. Letters 14, 142 (1965).

25) R.D. Macfarlane, Ark. Fys. 36, 431 (1967).

26) V.A. Karnaukhov and G.M. Ter-Akopyan, Ark. Fys. 36, 419 (1966).

27) P. Hornshøj, K. Wilsky, P.G. Hansen, B. Jonson, E. Kugler, M. Alpsten, Å. Appelqvist, G. Andersson, B. Bengtsson and O.B. Nielsen, Proc. Internat. Conf. on the Properties of Nuclei far from the Region of Beta Stability, Leysin, 1970 (CERN 70-30, 1970), Vol. 1, p. 487.

28) H. Schmeing, J.C. Hardy, R.L. Graham, J.S. Geiger and K.P. Jackson, Phys. Letters 44B, 449 (1973).

29) C.N. Davis and D.R. Gooseman, Phys. Rev. C 8, 1029 (1973).

30) P. Hornshøj, K. Wilsky, P.G. Hansen and B. Jonson, Nuclear Phys. A187, 637 (1972).

31) G.N. Flerov, V.A. Karnaukhov, G.M. Ter-Akopyan, L.A. Petrov and V.G. Subbotin, Nuclear Phys. 60, 129 (1964).

32) V.A. Karnaukhov, G.M. Ter-Akopyan, L.S. Vertogradov and L.A. Petrov, Soviet J. Nuclear Phys. 4, 327 (1966).

33) V.A. Karnaukhov, G.M. Ter-Akopyan, L.S. Vertogradov and L.A. Petrov, Nuclear Phys. A90, 23 (1967).

34) V.A. Karnaukhov, D.D. Bogdanov and L.A. Petrov, Proc. Internat. Conf. on the Properties of Nuclei far from the Region of Beta Stability, Leysin, 1970 (CERN 70-30, 1970), Vol. 1, p. 457.

35) D.D. Bogdanov, V.A. Karnaukhov and L.A. Petrov, Soviet J. Nuclear Phys. 17, 233 (1973).

36) D.D. Bogdanov, V.A. Karnaukhov and L.A. Petrov, Soviet J. Nuclear Phys. 18, 1 (1974).

37) D.D. Bogdanov, I. Bacso, V.A. Karnaukhov and L.A. Petrov. Soviet J. Nuclear Phys. 6, 807 (1968).

38) I. Bacso, D.D. Bogdanov, Sh. Darotsi, V.A. Karnaukhov and L.A. Petrov, Soviet J. Nuclear Phys. 7, 689 (1968).

39) D.D. Bogdanov, Sh. Darotsi, V.A. Karnaukhov, L.A. Petrov and G.M. Ter-Akopyan, Soviet J. Nuclear Phys. 6, 650 (1968).

40) V.A. Karnaukhov, Soviet J. Nuclear Phys. 10, 257 (1970).

41) E. Hagberg, P.G. Hansen, B. Jonson, B.G.G. Jørgensen, E. Kugler and T. Mowinckel, Nuclear Phys. A208, 309 (1973).

42) P. Hornshøj, K. Wilsky, P.G. Hansen, B. Jonson and O.B. Nielsen, Proc. Internat. Conf. on Heavy Ion Physics, Dubna, 1971 (Dubna report D7-5769, 1971), p. 249.

43) P. Hornshøj, K. Wilsky, P.G. Hansen, B. Jonson, M. Alpsten, G. Andersson, Å. Appelqvist, B. Bengtsson and O.B. Nielsen, Phys. Letters 34B, 591 (1971).

44) P. Hornshøj, K. Wilsky, P.G. Hansen, B. Jonson and O.B. Nielsen, Nuclear Phys. A187, 599 (1972).

45) E. Hagberg, P.G. Hansen, P. Hornshøj, B. Jonson, S. Mattsson and P. Tidemand-Petersson, to be published.

46) B. Jonson, P.G. Hansen, P. Hornshøj and O.B. Nielsen, Proc. Internat. Conf. on Nuclear Physics, Munich, 1973 (North-Holland, Amsterdam, 1973), Vol. 1, p. 690.

47) H.L. Ravn, Proc. Internat. Conf. on Reactions Between Complex Nuclei, Vanderbilt, 1974 (North-Holland, Amsterdam, 1974), Vol. 1, p. 194.

48) D.D. Bogdanov, A.V. Dem'yanov, V.A. Karnaukhov and L.A. Petrov, Soviet J. Nuclear Phys. 21, 123 (1975).

49) D.D. Bogdanov, J. Voboril, A.V. Dem'yanov, V.A. Karnaukhov, O.K. Nefediev and L.A. Petrov, Dubna report P6-8962 (1975).

50) D.D. Bogdanov, V.A. Karnaukhov and L.A. Petrov, Soviet J. Nuclear Phys. 19, 481 (1974).

51) D.D. Bogdanov, J. Voboril, A.V. Dem'yanov, V.A. Karnaukhov, L.A. Petrov, A. Plochocki and V.G. Subbotin, These proceedings.

52) P. Hornshøj, K. Wilsky, P.G. Hansen, B. Jonson, Phys. Letters 55B, 53 (1975).

53) J. D'Auria, J.W. Grüter, E. Hagberg, P.G. Hansen, B. Jonson, S. Mattsson and P. Tidemand-Petersson, to be published.

54) For references, see J.C. Hardy, Nuclear Data Tables 11, 327 (1973).

55) C.M. Lederer, J.M. Hollander and I. Perlman, Table of Isotopes (Wiley and Sons, Inc., New York, 1967).

56) V.A. Karnaukhov, D.D. Bogdanov, A.V. Dem'yanov, G.I. Koval and L.A. Petrov, Nuclear Instrum. Methods 120, 69 (1974).

57) K. Takahashi, M. Yamada and T. Kondoh, Nuclear Data Tables 12, 101 (1973).

58) The ISOLDE Collaboration, Phys. Letters 28B, 415 (1969).

59) The UNISOR Collaboration, Paper presented at the 24th Annual Nat. Conf. of the Academy of Sci. USSR on Nuclear Spectroscopy and Structure of the Atomic Nucleus, Kharkov, January 1974.

60) P. Hornshøj, K. Wilsky, P.G. Hansen, B. Jonson and O.B. Nielsen, Nuclear Phys. A187, 609 (1972).

61) K. Bos, N.B. Gove and A.H. Wapstra, Z. Phys. 271, 115 (1974).

62) A. Luuko, A. Kerek, I. Rezanka and C.J. Herrlander, Nuclear Phys. A135, 49 (1969).

63) L. Tomlinson, Nuclear Data Tables 12, 179 (1973).

64) S. Shalev and G. Rudstam, Phys. Rev. Letters 28, 687 (1972).

65) H. Franz, J.-V. Kratz, K.-L. Kratz, W. Rudolph, G. Herrman, F.M. Nuh, S.G. Prussin and A.A. Shihab-Eldin, Phys. Rev. Letters 33, 859 (1974).

66) S. Shalev and G. Rudstam, Nuclear Phys. A230, 153 (1974).

67) S. Shalev and G. Rudstam, Nuclear Phys. A235, 397 (1974).

68) K.-L. Kratz, W. Rudolph, H. Ohm, H. Franz, C. Ristori, M. Zendel, G. Herrman, F.M. Nuh, D.R. Slaughter, A.A. Shihab-Eldin and S.G. Prussin, These proceedings.

69) G. Rudstam and E. Lund, Phys. Rev. C 13, 321 (1976).

70) H.L. Ravn, Private communication, 1976.

71) V.I. Kuznetsov, N.K. Skobelev and G.N. Flerov, Soviet J. Nuclear Phys. 4, 202 (1967).

72) V.I. Kuznetsov, N.K. Skobelev and G.N. Flerov, Soviet J. Nuclear Phys. 5, 191 (1967).

73) V.I. Kuznetsov and N.K. Skobelev, Soviet J. Nuclear Phys. 5, 810 (1967).

74) N.K. Skobelev, Soviet J. Nuclear Phys. 15, 249 (1972).

75) C.O. Wene, Astron. and Astrophys. 44, 233 (1975).

76) C.O. Wene and S.A.E. Johansson, Phys. Scripta 10A, 156 (1974).

77) C.O. Wene and S.A.E. Johansson, These proceedings.

78) A.C. Pappas and T. Sverdrup, Nuclear Phys. A188, 48 (1972).

79) A.H. Wapstra and N.B. Gove, Nuclear Data Tables 9, 267 (1971).

80) W.D. Myers and W.I. Swiatecki, UCRL-11980 (1965).

81) C. Ekström, S. Ingelman, G. Wannberg and M. Skarestad, These proceedings.

82) H.J. Kluge, These proceedings.

83) K. Takahashi, Progr. Theor. Phys. 47, 1500 (1972).

84) B.G.G. Jørgensen, Forsinkede protoner fra beta-henfald af neutronfattige kerner, Cand. scient. thesis (Institute of Physics, Aarhus University, Denmark, 1974).

85) P.O. Martinsen and J. Randrup, Nuclear Phys. A195, 26 (1972).

86) J. Randrup, Nuclear Phys. A207, 209 (1973).

87) S.P. Ivanova, A.A. Kuliev and D.I. Salamov, Abstract, Cargèse, 1976.

88) P. Morrison, *in* Experimental nuclear physics (ed. E. Segrè) (Wiley and Sons, Inc., New York, 1953), Vol. II, p. 50.

89) F.D. Becchetti Jr. and G.W. Greenless, Phys. Rev. 182, 1190 (1969).

90) A. Arima, H. Horiuchi, K. Kubodera and N. Takigawa, Advances in Nuclear Phys. 5, 479 (1972).

91) P.G. Hansen, Proc. Internat. Conf. on Nuclear Structure and Spectroscopy, Amsterdam, 1974 (eds. H.P. Blok and A.E.L. Dieperink) (Scholar's Press, Amsterdam, 1974), p. 662.

92) Yu.P. Popov, *in* Nuclear Structure Study with Neutrons, Budapest, 1972 (eds. J. Erö and J. Szücs) (Plenum Press, London, 1974), p. 65.

93) G. Igo, Phys. Rev. 115, 1665 (1959).

94) J.O. Rasmussen, Phys. Rev. 113, 1593 (1959).

95) J.E. Lynn, The theory of neutron resonance reactions (Clarendon Press, Oxford, 1968): a) p. 180, b) p. 210, c) p. 319, d) p. 228.

96) C. Porter, Statistical theories of spectra (Academic Press Inc., New York and London, 1965).

97) P.G. Hansen, P. Hornshøj and B. Jonson, Abstract, Cargèse, and to be published.

98) G. Andersson, M. Asghar, A. Emsallem, E. Hagberg and B. Jonson, Phys. Letters 61B, 234 (1976).

99) D.R. Slaughter, F.M. Nuh, A.A. Shihab-Eldin and S.G. Prussin, Phys. Letters 38B, 22 (1972).

100) F.M. Nuh, D.R. Slaughter, S.G. Prussin, K.-L. Kratz, H. Franz and G. Herrman, Phys. Letters 53B, 435 (1975).

101) H. Tovedal and B. Fogelberg, Nuclear Phys. A252, 253 (1975).

102) A.M. Lane and J.E. Lynn, Proc. Phys. Soc. A 70, 557 (1957).

103) P. Axel, Symp. on Nuclear Structure, Dubna, 1968 (IAEA, Vienna, 1968), p. 299.

104) P.A. Moldauer, Phys. Rev. 123, 968 (1961).

105) J.C. Hardy, These proceedings.

106) P.G. Hansen, *in* Nuclear Structure (ed. V.G. Soloviev), Proc. Internat. School on Nuclear Structure, Alushta (USSR), 1972 (JINR-D-6465, 1972), p. 365-397.

107) V.A. Karnaukhov, D.D. Bogdanov and L.A. Petrov, Nuclear Phys. A206, 583 (1973).

108) S.O. Rice, Mathematical analysis of random noise, Bell Syst. Tech. J. 23 and 24 (1944-45).

109) A. Bohr and B.R. Mottelson, Nuclear structure (Benjamin Inc., New York, 1969), Vol. I: a) p. 155, b) p. 187.

110) E. Erba, U. Facchini and E. Saetta-Menichella, Nuovo Cimento 22, 1237 (1961).